JOHANNES KEPLER
UNIVERSITÄT LINZ

Author
Bahareh Attar
K11811449

Biochemical analysis of Orai1 mutants derived from a cancer database

Submission
Institute for Biophysics

Thesis Supervisor
Dr.in Irene Frischauf

Head of Laboratory
Dr. Christoph Romanin

Bachelor's Project

to confer the academic degree of Bioinforatic

Oct 2022

Bahareh, A., 2023: Biochemical analysis of Orai1 mutants derived from a cancer database. BC. Thesis, in English. 57 p., Faculty of Science, University of South Bohemia, České Budějovice, Czech Republic.

Annotation:

This thesis presents a comprehensive biochemical analysis of Orai1 mutants sourced from a cancer database, providing valuable insights into their functional characteristics. Utilizing PyMOL, the 3D structures of the Calcium release-activated calcium (CRAC) channel ORAI and its K163W mutant were visualized in the closed channel state, shedding light on their conformational properties. Furthermore, the study focused on investigating the open conformation of the CRAC channel Orai. Notably, the H206A gain-of-function mutation, which has implications in Drosophila melanogaster, was thoroughly examined in these three variants. To enrich the findings, the research references relevant literature and employs chemical detection methods to compare the closed and open channel states in both human and Drosophila species, deepening our understanding of the functional dynamics of these channels.

STATUTORY DECLARATION

I declare that I am the author of this qualification thesis and that in writing it I have used the sources and literature displayed in the list of used sources only.

Acknowledgements

First and foremost, I would like to thank my co-supervisor Dr. Irene Frischauf for her patient guidance, helpful advice, and direction. I thank her for all her support, help and expert opinions.

I would like to thank Professor Christoph Romanin for being my supervisor and giving me the opportunity to write this bachelor thesis in the biophysics group. I thank him for his continuous support, enthusiastic encouragement and all his advice. Working in the biophysics group was a great experience that gave me a lot of knowledge about ion channels and Orai1.

Most of all, I would like to express my deep gratitude to my family and my husband for their love and encouragement during my studies and beyond. Thank you for supporting me always and in so many ways that I cannot even attempt to list them here.

Abstract:

Calcium is a crucial ion in the human body and plays many vital functions. One of its important roles is as a component of the plasma membrane in cells. The depletion of endoplasmic reticulum (ER) stores triggers the activation of Ca^{2+} release-activated Ca^{2+} channels (CRAC), which rely on two key proteins, STIM1 and Orai1. STIM1, a Ca^{2+} sensor located in the ER, undergoes a conformational change and translocates to the ER-PM junctions where it activates Orai1, the pore-forming subunit in the plasma membrane. This results in the opening of the CRAC channel, allowing Ca^{2+} ions to enter the cell.

A CRAC channel functions like a team of six Orai1 subunits. These subunits open and close thanks to specialized components known as transmembrane domains (TM). When the channel becomes active, these domains must move or rotate to allow Ca^{2+} ions to enter. This study closely examines two types of modifications in the Orai1 channel that are associated with cancer: one known as R91C on its own, and another referred to as H134A+R91C (where R91C is altered). These modifications resemble differences in the channel's behavior. The investigation utilizes information from 4HKR and 4HKS, which showcase the closed channel state similar to the regular human Orai channel. Additionally, PyMOL analysis involving 6BBF is employed, revealing the open channel state akin to the H134A+R91C alteration in humans. Through these tools, the study gauges the extent to which a component named K163W shifts when the channel transitions from being closed to being open.

The objective of this study involves employing PyMOL, along with pertinent references, to explore the chemiluminescence detection mechanism of membranes featuring the H134A+R91C mutation and the R91C mutation in humans. This investigation extends to a comparative analysis with the closed-channel 4HKS(K163W) mutation observed in Drosophila melanogaster, which shares similarities with the R91W mutation in humans. Additionally, the study encompasses the open-channel 6BBF (H206A) mutation in Drosophila melanogaster, akin to the H134A+R91C mutation in humans. Through these analyses, a deeper understanding of the chemiluminescence properties of these mutations across species can be gained.

Figure Index:

Contents:

1. Introduction

1.1 Ion Channels:

Ion channels are special protein molecules that span the cell membrane, acting like tiny gates(90). These gates allow specific ions to move across the membrane, playing important roles in various bodily processes like hormone release, cell growth, and maintaining balance in our body fluids(57). Sometimes, when these channels become dysfunctional or mutated, they can cause disorders known as channelopathies(57). What makes ion channels unique is that they have two important features(9). First, they can be selective, allowing only certain ions to pass through a filter, which controls the speed of ion movement. Second, they are "gated," which means they can change shape and open up to allow ions to pass through(102).The correct positioning of cell volume and the presence of ion channels and transporters within the intercellular environment are crucial for the migration of the machine cytoskeleton. These ion channels and transporters play a vital role in regulating and facilitating the migration of different cell types(103).

1.2. Calcium (Ca^{2+}):

Calcium (Ca^{2+}) is really important in eukaryotic cells. It helps regulate a lot of cellular activities by carefully controlling where and when it's present (1). Different parts of the cell, like neurons, have special places where they store calcium inside, such as the endoplasmic reticulum, mitochondria, or nuclear envelope (2, 3). These storage spots are like mini warehouses that allow the cell to adjust the amount of calcium as needed(2). This helps the cell perform specific tasks and keeps everything in balance, which is crucial for its overall well-being(1,3).

External stimuli influence intracellular calcium levels, impacting diverse biological processes. Calcium (Ca^{2+}) directly or indirectly regulates exocytosis, contraction, metabolism, transcription, fertilization, proliferation, vision, memory, and immune response. As a vital messenger, Ca^{2+} plays a central role in transmitting signals between and within cells, facilitated by multiple molecular mechanisms(4).

When ATP is used as an energy source inside cells, it requires only a small amount of calcium (Ca^{2+})(4). It is vital for cells to maintain low levels of free calcium within them to survive(5). To achieve this, a calcium homeostatic system has evolved, which regulates the movement of calcium across cell membranes and maintains a balance between calcium entering and leaving the cell. This

system consists of various molecular processes that control the levels of calcium in the cytoplasm (known as Ca^{2+} buffer) and transport excess calcium out of the cell using calcium transporters(6). This homeostatic system is essential for calcium signaling, as the difference in calcium concentration between the outside and inside of cells allows calcium to diffuse through membrane channels(5). Calcium-binding proteins interact with enzymes and other molecules to interpret, amplify, and transmit calcium signals, playing a critical role in the positive and negative feedback of calcium transport(2,6). This enables cells to generate rapid changes in local calcium levels, referred to as spikes and waves(2). The endoplasmic reticulum (ER) acts as an internal calcium storage, which is crucial for creating temporary changes in cytosolic calcium levels(1). The ER lumen contains a calcium concentration that is at least two orders of magnitude higher than the cytoplasm (Figure 1), allowing for rapid signal transduction to the cytosol with low energy cost(1,7). A reduction in calcium storage in the ER would be detrimental, as many essential calcium-dependent processes, such as protein folding, degradation, chaperone activity, vesicle transport, lipid and steroid biosynthesis, occur in the ER lumen (7).

Despite the significant size of the ER in cells, there is a more constant supply of the signaling ion, calcium (Ca^{2+}), in the extracellular medium(7). This maintains calcium levels several orders of magnitude higher in the extracellular medium compared to the cytosol (i.e., about 1-2 mM) (Figure 1), similar to the flux of ER luminal calcium. The exchange of extracellular calcium with the cytoplasm is necessary because sustained high intracellular calcium levels can be cytotoxic and lead to apoptosis and necrosis (7).

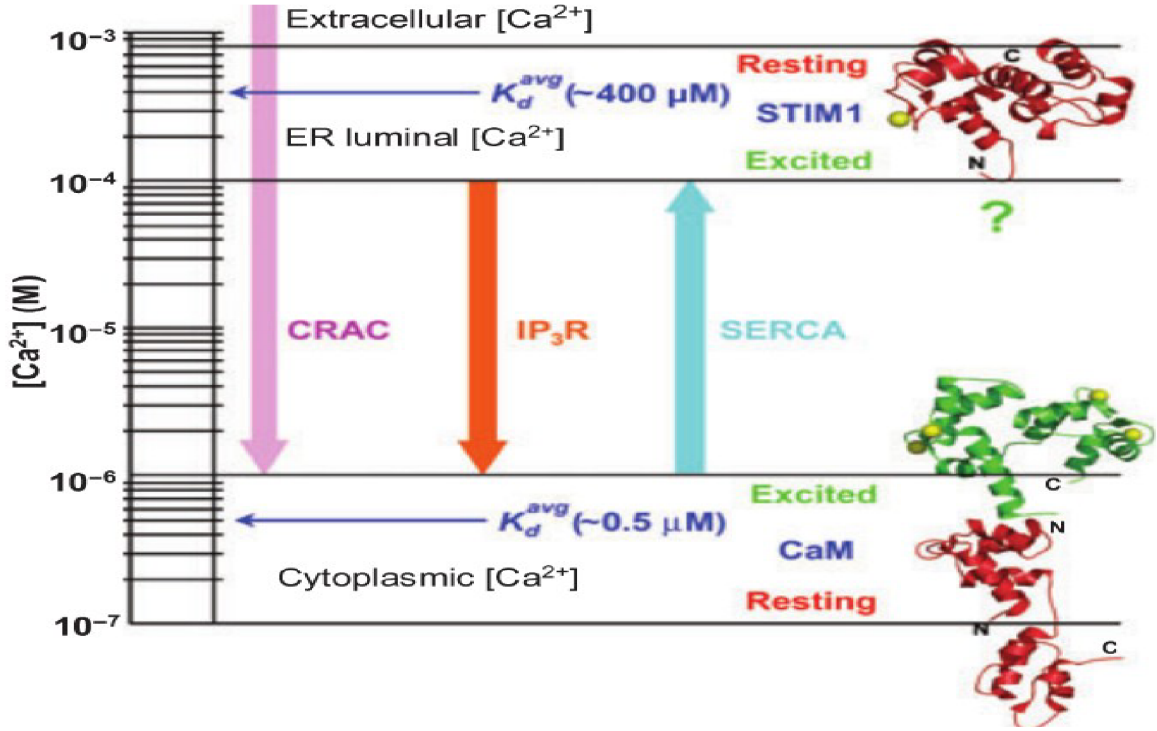

Figure. 1.The graph illustrates Ca^{2+} exchange in store-operated Ca^{2+} entry (SOCE) and calcium release-activated calcium (CRAC) entry. Cytoplasmic Ca2+ regulates CaM activity. ER sensors activate upon luminal Ca^{2+} depletion.

IP3 receptors and CRAC channels mediate Ca^{2+} flux, while SERCA pumps refill ER. SOCE replenishes ER and boosts cytoplasmic Ca2+ for cellular responses.

Ca^{2+} flux involves ion channels, pumps, exchangers, buffers, and sensors that regulate localized Ca^{2+} signals in cells(2). Store-operated Ca^{2+} entry (SOCE) is the primary mechanism for increasing cytoplasmic Ca^{2+} levels in eukaryotes(6). SOCE is triggered when ER Ca^{2+} stores are depleted, causing plasma membrane Ca^{2+} channels to open(2). This sustained increase in Ca^{2+} plays a critical role in cellular responses such as transcriptional activation and replenishing ER stores(5).
In lymphocytes, store-operated Ca^{2+} entry (SOCE) through CRAC channels in the plasma membrane increases cytosolic Ca^{2+} levels(8,9). Impaired sustained Ca^{2+} influx in CRAC channels leads to minor immunodeficiency diseases, affecting lymphocyte functions(8). T and B lymphocytes activate phospholipase Cg, producing IP3, which binds to ER receptors, triggering Ca^{2+} release and initiating SOCE. CRAC import supplies cytoplasmic Ca^{2+} for cytokine release and immune replication(9). Transient receptor potential (TRP) channels respond to stimuli, mediating cation influx, except TRPM4 and TRPM5, which are impermeable to Ca^{2+}(10). Store-operated calcium channels (SOCS) are activated by ER Ca^{2+} depletion and serve as the main pathway for calcium signal transduction(15).

1.3. CRAC (calcium release activated calcium) channel:

One group of store-operated calcium channels (SOCs) in the plasma membrane is the CRAC channel, which has been identified in mast cells and T cells using patch clamp and calcium imaging techniques (16,17). SOCs are the primary pathway for calcium signaling in non-excitable cells of metazoans, and CRAC channels are activated by store-operated calcium entry (SOCE) (18,19) (Figure 2). The mechanism of SOCs involves an extracellular agonist binding to a cell-surface receptor, triggering a G-protein or tyrosine kinase cascade that activates phospholipase C (PLC). PLC cleaves phosphatidylinositol 4,5-bisphosphate (PIP2) to generate inositol 1,4,5-trisphosphate (IP3) (19). IP3 binds to its cognate receptor, a tetrameric protein on the ER, and acts as a calcium channel. The IP3 receptor senses the cytosolic calcium concentration and signals the ER to release calcium, controlling the CRAC channel and causing calcium influx into the cell (12,15,19). The CRAC channel consists of two key components, STIM1 and Orai1 (18,22). STIM1 is a transmembrane protein in the ER that functions as a sensor of the luminal calcium concentration (20). Orai1 is a plasma membrane protein that forms the pore of the CRAC channel (19,21). The release of calcium stores leads to the interaction of STIM1 and Orai1, activating the channel and resulting in the influx of calcium into the cytosol (22,23).

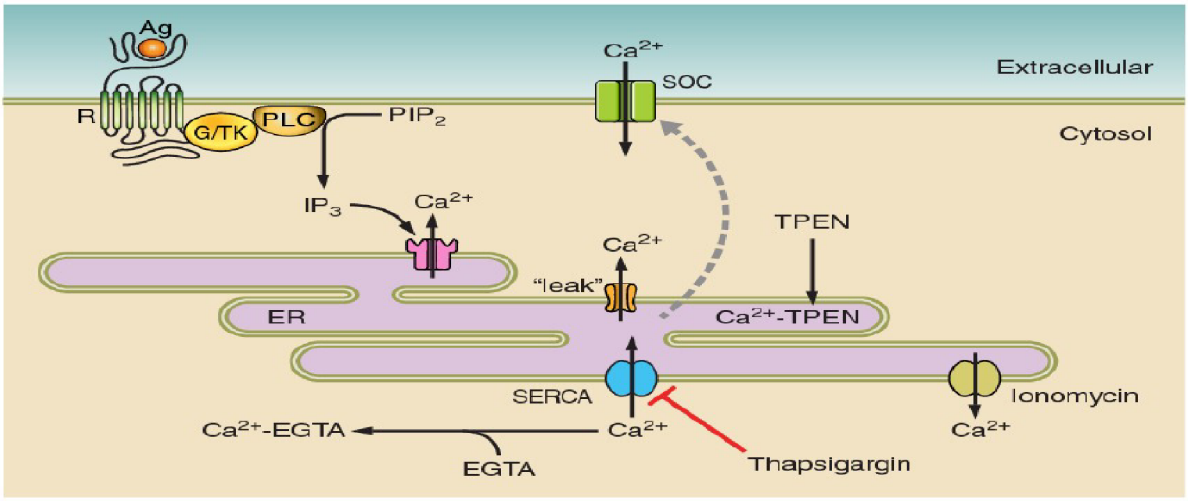

Figure 2: Store-operated Calcium Entry (SOCE). The illustration depicts SOCE activation through various methods, including chelating intracellular Ca^{2+} with EGTA, inhibiting SERCA pumps with thapsigargin, releasing Ca^{2+} from the endoplasmic reticulum with ionomycin, or chelating intraluminal Ca^{2+} with TPEN (15).

1.4. Paradigm of intracellular Ca^{2+} sensing:

Intracellular Ca^{2+} sensors are proteins that undergo conformational changes in response to Ca^{2+} binding or release and mediate specific cellular and biomolecular functions (24,27). These sensors differ from protein buffers, which regulate local Ca^{2+} levels by binding or releasing Ca^{2+}, and from pumps and exchangers, which transport Ca^{2+} between compartments and are usually compact in structure (24).The largest intracellular Ca^{2+} sensor proteins contain the well-known EF-hand Ca^{2+}-binding motif, first observed at the atomic level in the parvalbumin crystal structure (24). The EF-hand motif is composed of a helix-loop-helix architecture with a 12-amino acid interhelical loop that coordinates a single Ca^{2+} ion. In general, a single structural component comprises a pair of EF-hand motifs for increased structural stability and Ca^{2+} sensitivity (25,26).The most important Ca^{2+} sensor for various signaling processes is calmodulin (CaM), which is highly conserved from roundworms to humans (27)

Calmodulin (CaM) consists of 148 residues and encodes two EF-hand domains linked by a flexible central linker. Its four binding loops exhibit high affinity and cooperativity for Ca^{2+} (Kd around 0.1-1 μM) (28).Most Ca^{2+}-sensing proteins, including CaM, contain four motifs such as DREAM and Ca^{2+}-binding protein 1, while some sensors contain only one pair, such as proteins and nucleobindin. All Ca^{2+}-sensing proteins carry out their functions in the cytoplasm or nucleus (28,29)

There are two structural features of CaM that contribute to its promiscuity: First, the central helix connecting the two EF-hand domains has a flexible portion (residues 78-81) that can bend dramatically, allowing each domain to shift independently and coordinate with its target. Second, the hydrophobic cleft of each domain is rich in methionine residues, which provide local flexibility for tight interactions with hydrophobic residues (20, 29)

Several proteins are involved in activating T-cells and are regulated by CaM interactions in the cytosol, including calcineurin phosphatase, IP3 receptor anchored on the ER membrane, CaM kinase II, and CaM kinase IV (30). CaM plays a significant role in the cytosolic interaction of both STIM1 and STIM2 in cell culture and in vitro (31,32). As a cytosolic Ca^{2+} sensor, CaM can respond to changes in Ca^{2+} signals such as spikes, waves, and fluctuations in the cytoplasm. CaM has a high affinity and cooperativity for binding Ca^{2+}, which increases its sensitivity, allowing for a stronger bond with each subsequent Ca^{2+} ion(32). This precise response to Ca^{2+} binding, enabled by the cooperativity of Ca^{2+}, gives CaM a strong molecular on-off switch function (Fig. 1)(29).

The presence of low levels of Ca^{2+} in the cytosol calls for a sophisticated mechanism for Ca^{2+} binding in cytosolic sensor proteins. By studying compartmentalized Ca^{2+} sensing, where the levels of Ca^{2+} are maintained at a higher order of magnitude compared to the cytosol, researchers have gained a better understanding of the sensing mechanisms within the ER lumen, as demonstrated by the example of STIM1. The data available indicates that STIM1 represents an archetypal ER Ca^{2+} sensor, exhibiting similarities as well as distinct differences when compared to cytosolic sensors like CaM, emphasizing the diversity of this crucial group of Ca^{2+}-binding proteins (30).

1.5. STIMs as ER-specific Ca^{2+} sensors:

The presumptive STIM domains based on their sequences: Human STIM1 is a 685 amino acid protein that is a type I transmembrane protein with its C-terminal domains located in the cytoplasm (as shown in Fig. 3). Although a small portion of STIM1 has been identified on the plasma membrane, the majority of it is located on the ER membrane, with its N-terminal domains positioned in the extracellular space or the ER lumen (11, 33, 34). The N-terminal sequence of the protein contains localization signals, such as those for the ER and a single EF-hand motif, as well as a sterile alpha-motif (SAM) domain (32, 35).

The N-terminal domains and C-terminal domains of STIM1 are separated by a single transmembrane segment (37). The cytoplasmic domains of STIM1 contain two coiled-coil regions, which are suspected based on the sequence. These two regions are not present in the ezrin-radixin-moesin (ERM) domain. The C-terminal side of the protein is comprised of a Lys-rich domain and a

Pro/Ser-rich region, and phosphorylation takes place at various Ser and Thr sites within the Pro/Ser-rich region (38).

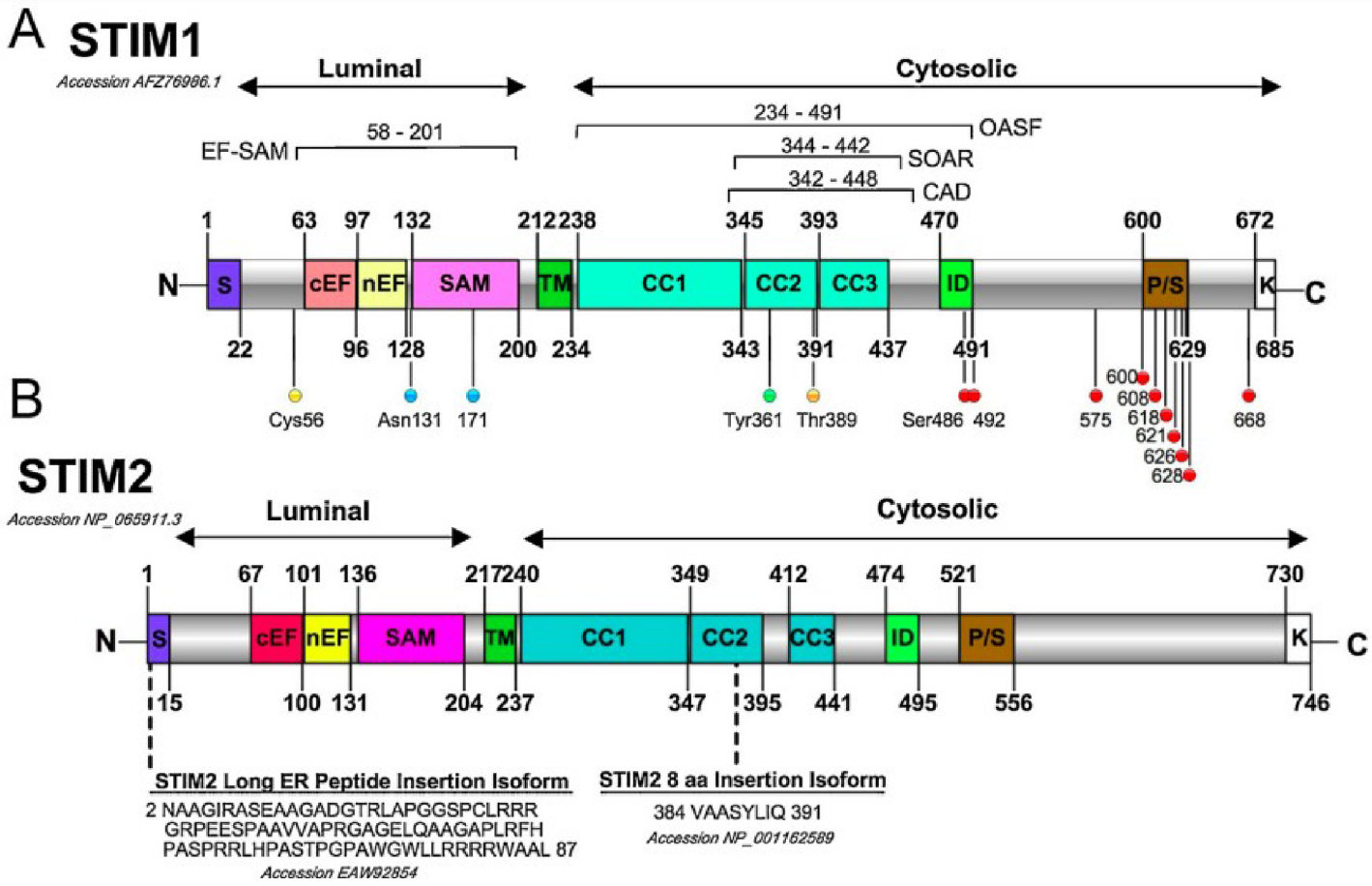

Figure 3: This figure illustrates the architecture of human STIM1 and STIM2 proteins. Part A depicts the domain structure of STIM1, highlighting different fragments used in structure-function studies. Posttranslational modifications are indicated with colored symbols below the diagram. Part B showcases the domain architecture of STIM2, with labeled residue regions and dashed lines indicating amino acid insertions for STIM2 isoforms. The cellular localization of the STIM region is shown at the top of both diagrams, with labels for various functional regions (38).

The second isoform, STIM2, is expressed in mammals and has a high degree of sequence similarity (greater than 65%) with STIM1 (as shown in Figures 2 and 3). The most notable differences between the human homologs are at the C-terminal, particularly the coiled-coil domains (39 ,41). Additionally, there is significant variability at the N-terminal end of the proteins. STIM2 appears to be restricted to the ER membrane, regardless of the presence of the conserved Asn131 glycosylation site (which is Asn135 in STIM2). This restricted localization may be due to the presence of a consensus ER-conservation signal in STIM2 (41). The EF-hand, SAM, coiled-coil, and ERM-likeCa^{2+} regions are the most conserved domains among vertebrates (40). The movement of STIM1

to the ER-PM junction facilitates the recruitment of the Orai1 component of the CRAC channel, which is necessary for the maintenance of SOCE/CRAC entry (42 ,43). The simultaneous expression of both STIM1 and Orai1 results in a significant increase in CRAC current, indicating that these two proteins are the molecular components responsible for the formation of the SOCE/CRAC input (14,43).

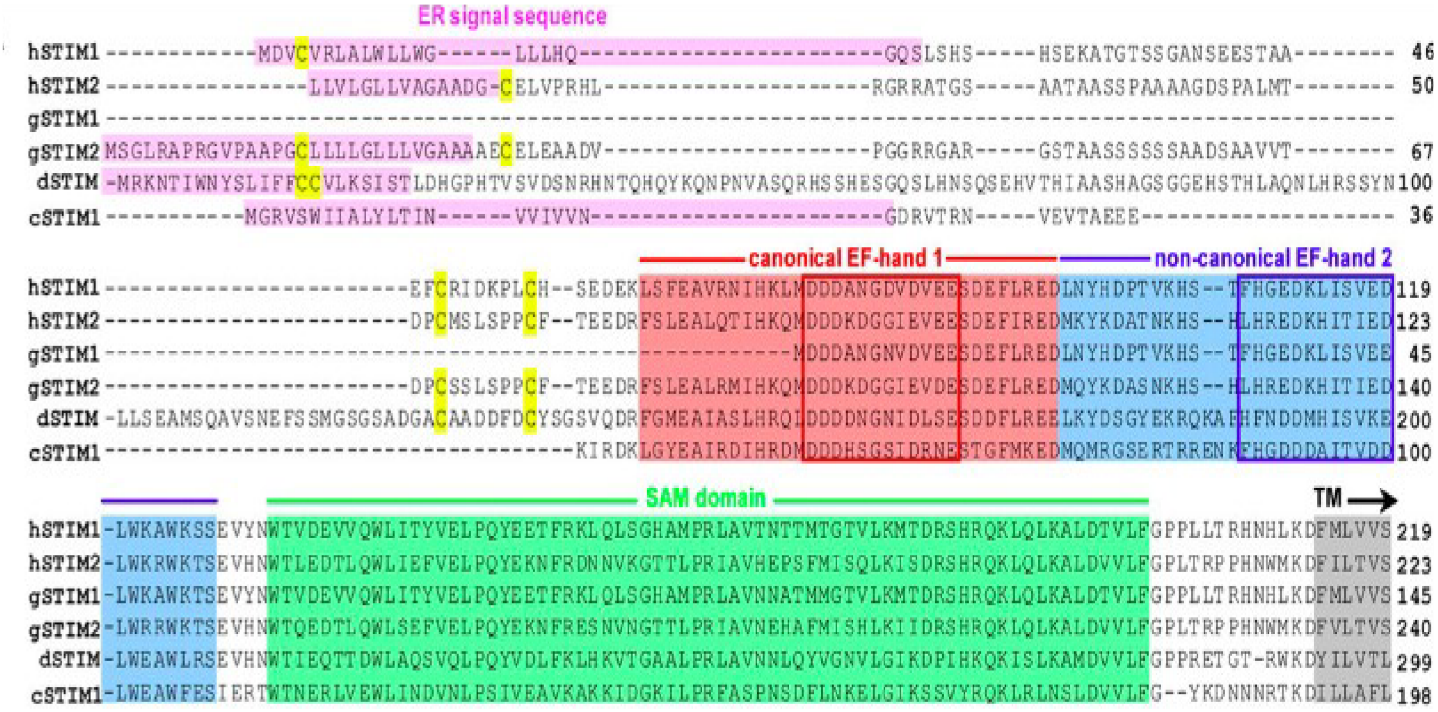

Figure 4: Sequence homology of EF-SAM and deployment rates. The diagram shows an alignment of the luminal domains of different STIM isoform sequences, using ClustalW for comparison of STIM1 and STIM2 from Homo sapiens, Gallus gallus, Drosophila melanogaster, and Caenorhabditis elegans. The purple shading represents the predicted ER signal sequence. The residues in the EF-hand 1 are shown in red, those in the non-canonical EF-hand 2 are in blue, the SAM domain is in green, and the predicted transmembrane is gray. The residues in the EF-hand loops are connected by boxes, and all cysteine residues are shaded yellow(39).

In cell biology experiments, altering a specific Ca^{2+} binding site within the EF-hand motif junctional loop disrupts the organization of punctate STIM1 oligomerization and its clustering with Orai1 at ER-PM junctions(41). This alteration also reduces the entry of Ca^{2+} through SOCE/CRAC channels due to impaired coordination of Ca^{2+} ions(13,28). Additionally, removal of the SAM domain renders STIM1 insensitive to Ca^{2+}, leading to the loss of punctate formation(44). The accumulation of STIM1 at ER-PM junctions upon ER Ca^{2+} depletion is crucial for activating CRAC channels(41). A notable experiment showed that replacing the EF-SAM domain with the FK506- and rapamycin-binding protein (FKBP12) or FKBP-rapamycin-binding (FRB) domain of the Mammalian Target of Rapamycin disrupted Ca^{2+} dependence. In cells expressing

STIM1-FRB/FKBP12 fusions, response to rapamycin influenced SOCE/CRAC entry, regardless of ER luminal Ca^{2+} levels(44).

1.6. Orai proteins:

The process of restoring Orai1 in mammals involved the use of a single nucleotide polymorphism array analysis and a RNA interference screen from Drosophila (45) (Figs. 5,6). The Orai protein, also known as the CRAC modulator or CRACM, opens the CRAC channel selectively to Ca^{2+} (46,47,48). The full-length human Orai1 is found in the plasma membrane along with its related proteins, Orai2 and Orai3 (49). The crystal structure of Orai from Drosophila melanogaster is similar to that of human Orai, with 73% sequence identity (50). The CRAC channel is made up of six Orai subunits arranged around an ion pore, with the subunits perpendicular to the plasma membrane (50). Each Orai1 subunit has four transmembrane helices (designated M1 to M4 or TM1 to TM4) and one M4 propagation helix. The dOrai1 monomers form three dimers, resulting in a triply symmetrical structure (50). These sections can be differentiated by a curved proline residue. The four transmembrane segments are connected by one intracellular and two extracellular loops, as well as NH2 and COOH termini on the cytosolic side (51) (Fig. 5A). The NH2 and COOH termini of Orai1 and Orai3 proteins show a sequence homology of 34% and 43%, respectively (52).

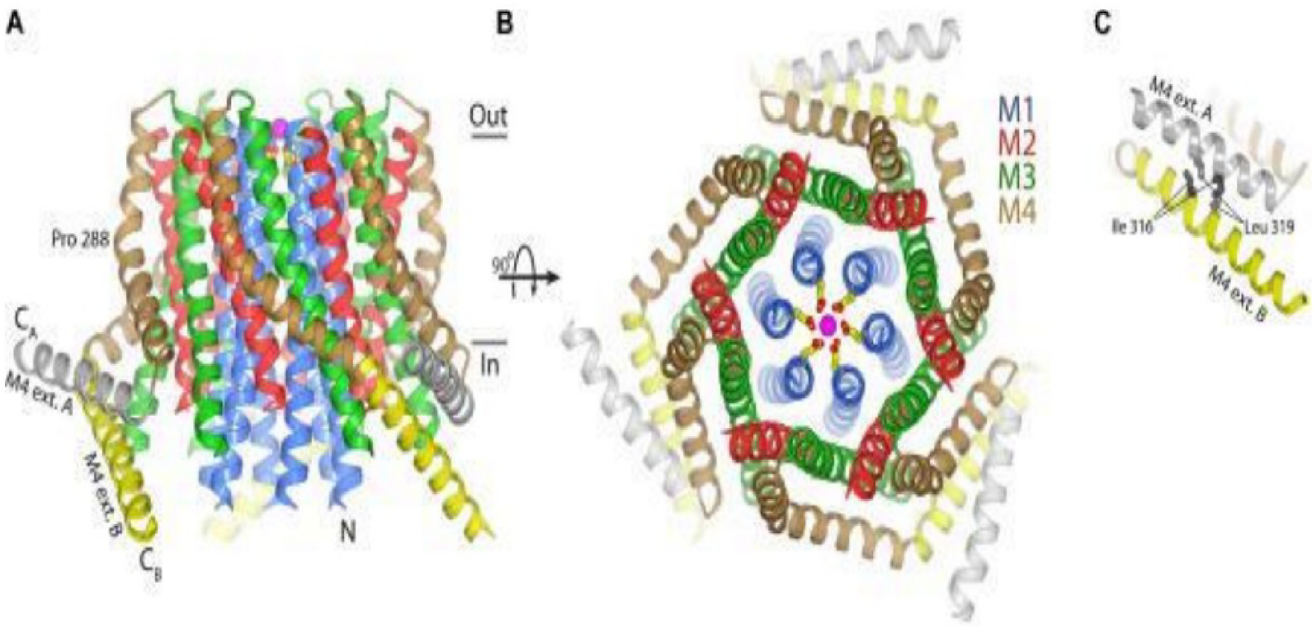

Figure 5: The design of Orai1 is depicted in three parts. Part A displays a side view of the channel's structure, Part B displays a top view of the same structure with a magenta sphere representing calcium ion, and Part C offers a close-up look at the interaction and response between the M4 helices as they unfold. (50).

Orai1 NH2 terminus:

The N-terminal end of Orai1, including the Expansion TM1 Orai1 N-terminal (ETON) region (aa73-90), is an extension of the TM1 that extends into the cytosol (51)(Fig. 6A). The three positively charged residues (R91, K87, and R83) in the TM1-ETON region form an electrostatic barrier that functions as a gate, controlling Ca^{2+} influx into the cytosol by preventing it from flowing in (52). STIM1-Orai1 pairs can remove this barrier, allowing Ca^{2+} to enter the cytosol (75). Mutations in K85, K87, and R91 result in a disruption of the Orai1-STIM1 interaction (54). Paired mutations in the ETON region, such as L74/W76, L74/L79, and L81/L86, reduce pairing and purification of Orai1 by STIM1 (53,54). S89 and S90, located between R91 and K87 in the ETON region, affect the flexibility of the adjacent N-terminal and TM1 segments. Replacing these residues with glycines results in increased helical flexibility and Orai flux(75).

The ETON region, including S89 and S90 located between R91 and K87, affects the flexibility of the neighboring N-terminal and TM1 segments. Replacing the serines with glycines leads to improved helical flexibility and Orai currents. However, the S98P and S90P mutations cause a decrease in function due to increased helical stiffness (55). As a result, the ETON region serves as a link and possible portal for STIM1-Orai1 interactions and reactions (56).

Orai1 COOH terminus: As demonstrated in Figure 5A, the COOH end of Orai1 serves as a robust binding site in comparison to the NH2 end in the STIM1 interaction (58). The organization of the cytosolic spread is managed by M4-Ext helices that connect the C-terminus to M4 via a highly conserved hinge (aa261-265) (Fig. 5B)(50). This hinge holds a critical role in linking Orai1 and STIM1 by impacting the composition of the COOH end of Orai1. A mutation in the hinge disrupts the STIM1 connection and CRAC activation (59). The Orai family also includes a coiled-coil domain in the COOH end, which is crucial for protein-protein interactions. Residues L273, L276, R281, L286, and R289 play a significant role in the interaction with the COOH end of STIM1's SOAP, and point mutations L273S/D and L276S also interfere with the STIM1 interaction (60,62). L273 and L276, being hydrophobic residues, are important for channel gating and Orai activation (61). The front junction of STIM1 is cleaved through cysteine cross-linking of the C-terminal pairs at these sites (62). In the COOH end of Orai2 and Orai3, colonic mutations entirely break the interaction with STIM1 (64).

The interaction between STIM1 and Orai1 is also largely dependent on both the NH2 and COOH termini of Orai1. Any mutation in these termini leads to the complete loss of Orai1 function (65). If the NH2 terminus is damaged, it affects the STIM1-Orai1 coupling and functionality, while a disrupted COOH terminus eliminates interaction with STIM1 (56). The sequence of events during the STIM1-Orai1 coupling is believed to be first binding of STIM1 to the binding sites in the COOH terminus followed by binding to the junctional sites in the NH2 terminus (65).

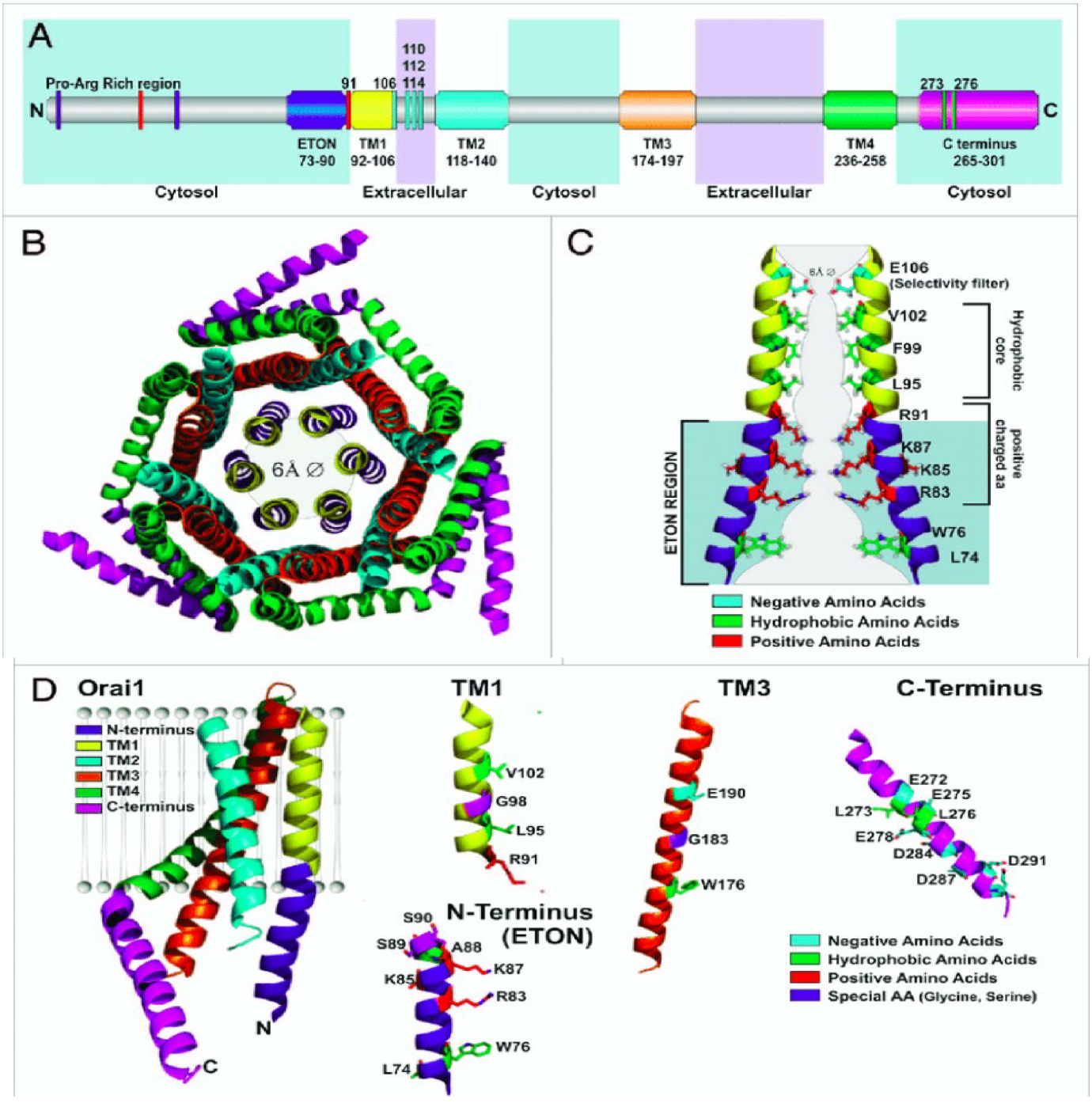

Figure 6: Orai1: (A) The full-length human Orai1 is displayed with the key residues that are crucial to its function. (B) The X-ray crystal structure of Drosophila Orai reveals that the six subunit transmembrane domains are arranged in concentric circles around the ion pore, with TM1 forming the innermost ring surrounding the ion pore. (C) The human Orai1 pore consists of two TM1 strands and cytosolic helical extensions that are part of the conserved eTON region. (D) A single Orai1 subunit is comprised of four transmembrane regions (TM), an N-terminus, and a C-terminus extended helices, displayed in different colors as seen in (A-D). The residues that are connected to the function of Orai1 are emphasized in separate depictions of TM1, TM3, the C-terminus, and the N-terminus, with the amino acid numbering referencing human Orai1 (53).

Orai1 gating:

The Orai1 ion channel remains closed, preventing calcium from entering the plasma membrane until it is activated (16). The stationary X-ray crystal structure of the channel shows that the path for translation consists of six TM1 segments located at the center of the Orai1 complex. This narrow and bound ion pore, which is 55 Å long, has four distinct regions: an external vestibule (50), the selectivity filter, and a hydrophobic cavity that extends into the cytosol via the basal region. The vestibule in the external area is made up of highly flexible TM1-TM2 loops, most of which contain three negatively charged residues: D110, D112, and D114 (50). These residues form the calcium condensation site in the Orai channels and capture calcium ions entering the pore (66). A single point mutation from D110 to alanine can decrease calcium leakage when there is a reduced concentration of extracellular calcium. This is because the mutation shifts the calcium binding site to D112 and D114 and affects the growth of the energy barrier between the selectivity filter and the calcium binding site (66). This suggests that negatively charged residues can lower the energetic barrier to calcium secretion. Interactions between the TM1-TM2 electrostatic loop and the TM3-TM4 junctional loop may also fine-tune the secretion of calcium into the pore. An alteration of disulfide bonds leads to an increase in store-operated current density, while cross-linking of cysteine at D112 and R210 has the opposite effect (67). This suggests that loop 3 is involved in regulating calcium influx by interacting with calcium at similar binding sites located on the extracellular side of the calcium condensation site(20). The replacement of residues in this loop also changes ion selectivity and makes the pore flatter. Orai1 has three glutamate residues in its first extracellular loop, while Orai2 and Orai3 have a combination of glutamate, glutamine, and aspartate residues. Once calcium ions are taken up by the negatively charged residues (D110, D112, D114), they pass through the selectivity filter on the extracellular side of TM1, which is composed of six glutamate residues at E106(41). Mutations of E106 to glutamine or alanine impair function, while the E106D mutation reduces calcium selectivity and widens the pores(66). Studies using cysteine cross-linking have shown that the E106 residues are closely positioned and that the TM1 (aa99-104) residues are strongly elongated, both of which enhance calcium coordination at E106(67).

It has been found that specific residues in the Orai channel, such as V102 and G98 in TM1, play a crucial role in maintaining the channel in a closed state. Any alterations to these residues, such as the substitutions V102A/C and G98D, result in the Orai channel becoming continuously active and losing its selectivity (44). The presence of STIM1 can influence the effect of these mutations on the Orai channel (67). For example, when STIM1 is present, the V102A/C substitution leads to high calcium selectivity and a narrow pore, whereas when STIM1 is absent, it results in low calcium selectivity and a wider pore(67). Another residue, L138 in the TM1-TM2 region, is thought to contribute to keeping the Orai channel closed. A mutation to L138F causes the channel to remain

active continuously and can result in a muscle disorder known as tubular. The closed ion pore of Orai1 prevents calcium from entering the plasma membrane until the channel is triggered(68). The X-ray crystal structure in a stationary conformation shows that the pathway for ion transport consists of six TM1s located in the center of the Orai1 complex(67). The bound, narrow ion pore is 55 Å in length and has four main regions: an external vestibule, the selectivity filter, and a hydrophobic cavity that extends into the cytosol through a basal region(67). The vestibule of the external part is composed of highly flexible TM1-TM2 loops, most of which contain three negatively charged residues: D110, D112, and D114(68). These residues form the calcium condensation site of Orai channels and attract calcium ions entering the pore(67). A single point mutation of D110 to alanine can reduce calcium leakage in conditions of low extracellular calcium condensation, as it shifts the calcium binding site to D112 and D114 and modifies the growth of the energy barrier between the selectivity filter and the calcium condensation site(67).Negatively charged residues reduce the energetic barrier to calcium secretion by the riase. Interactions between the TM1-TM2 loop and TM3-TM4 loop may also affect calcium secretion(66). Changes in disulfide bonds affect store-operated current densities. Cross-linking of cysteine at D112 and R210 decreases them, suggesting that loop 3 associates with calcium and regulates calcium influx. Substituting these residues also alters ion selectivity and changes the pore shape. Orai1 has three glutamate residues in the first extracellular loop, while Orai2 and Orai3 have a mixture of glutamate, glutamine, and aspartate(66). Calcium moves through the selectivity filter on the extracellular side of TM1 after being absorbed by negatively charged residues (D110, D112, D114)(67). Point mutation of E106 to glutamine or alanine impairs function, while the E106D mutation decreases calcium selectivity and widens the pore. The TM1 residues and the E106 residues are tightly positioned, favoring calcium coordination(58). The H134A mutation in TM2 leads to high calcium selectivity and inward currents, while residues in TM3 affect gating and selectivity(68). The P245 residue in TM4 helps maintain the closed state of the Orai1 channel, and changing it can cause a condition called stormorken disease(68).

1.7.The open conformation of Orai1 pore:

When calcium ions (Ca^{2+}) are removed from the endoplasmic reticulum (ER), a channel becomes active, and this triggers the opening of a pore (86).In a particular study (105), scientists added a genetic change (H206A mutation) to a Drosophila Orai. This alteration revealed an x-ray image showing that the pore of Orai expanded. This change in Drosophila, located in a specific part (TM2), is similar in function to a change (H134A mutation) in human Orai1 that enhances its activity. This modified Drosophila Orai now looks like the Orai channels activated by STIM (94) (101).When the channel is not active, a certain part of the Orai protein (His206) makes a connection

with another part (Ser165) (106). It's been suggested that, when the channel is active, this genetic change (H206A mutation) can fit into the regular Orai without causing any blockages(106). Using X-ray technology to see the structure, demonstrated that the open form of Orai1 has 24 pieces called subunits, grouped together to create four complete channels (Figure 7).

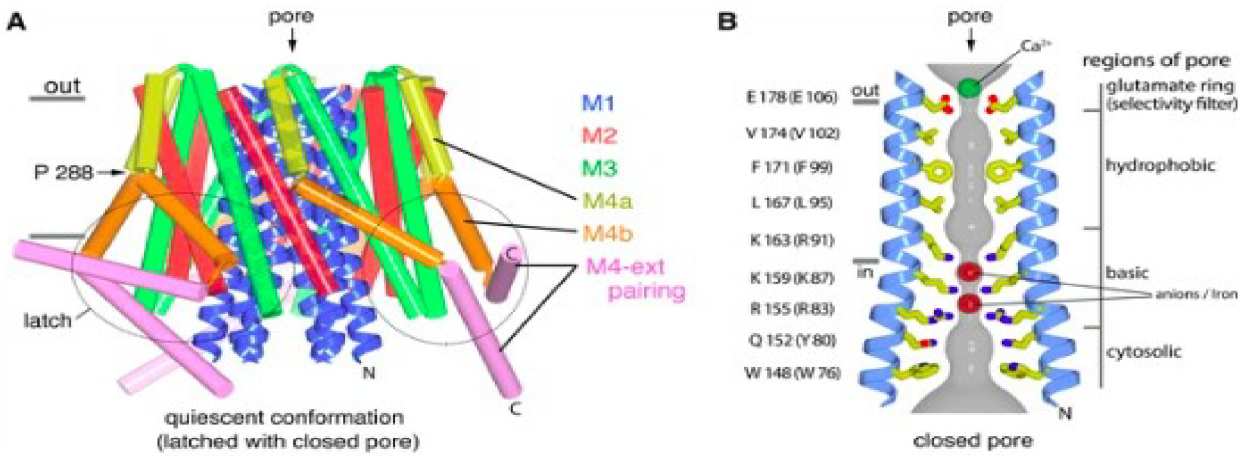

Figure 7: A Comprehensive View of Orai1 in its quiescent conformation(50).A:The channel is in a closed state, and the M4-ext helices are linked together. M1 helices are visualized using blue ribbons, while the remaining helices are represented as cylinders. The approximate limits of the membrane are indicated by gray bars, and regions referred to as 'latches' in this scenario are highlighted with dashed oval shapes(50).

B:The image offers a detailed look at the structure of the closed pore. Two M1 helices are depicted as ribbons, and the gray surface shows the closest distance to van der Waals contact. Amino acid side chains that shape the pore walls are illustrated as sticks, with colors representing carbon, nitrogen, and oxygen. Amino acid numbering is provided for Drosophila melanogaster Orai without parentheses and for human Orai within parentheses. Different parts of the pore are emphasized. While horizontal gray bars hint at the membrane's boundaries, M1 helices are shielded by M2 and M3. A Ca^{2+} ion is marked, and red spheres point to electron density connected with iron(50).

Inside this open channel, six subunits arrange themselves like the pattern of a beehive, forming a structure that surrounds the passage for ions(102). Just like when the channel is inactive, each subunit has four parts that cross the cell membrane (M1-M4), and these M1 parts protectively encircle the pore(102). The M4 parts are made up of two components, M4a and M4b, and the M4-ext part extends from M4b into the inside of the cell(102). The open Orai1 pore includes a filter made of six parts that only let certain ions pass (called glutamate or Glu106), along with other longer parts that are hydrophobic, basic, and part of the inside of the cell (102) (Figure 8A). Unlike when the pore is closed, the end of the pore inside the cell gets much wider, stretching about 10 units of measurement (angstroms) at a point called Lys159 (Figure 8)(102).

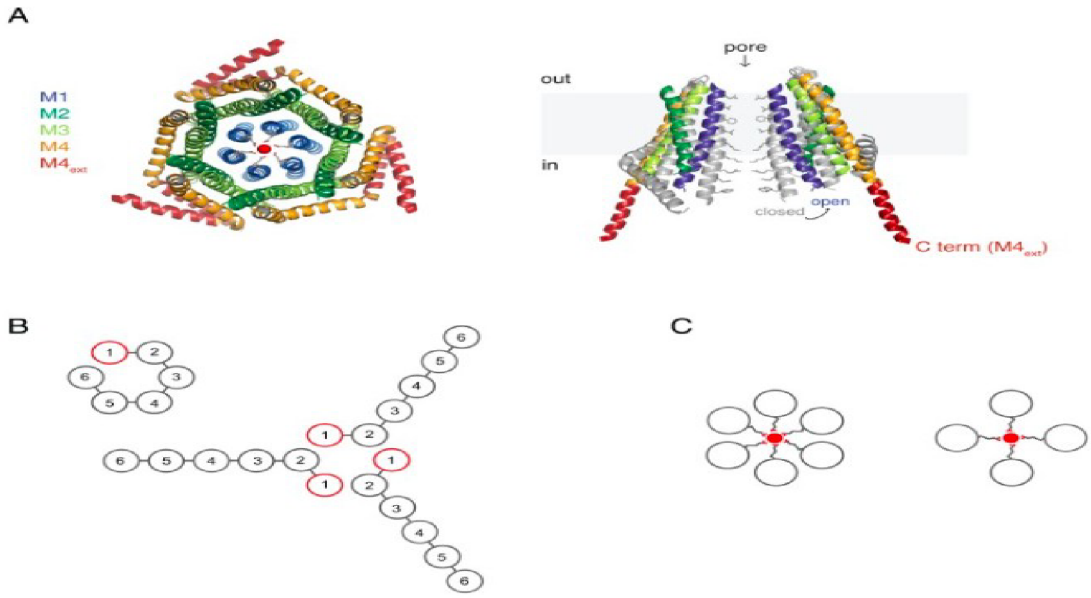

Figure 8: Unveiling the Open Configuration of the H206A Orai Structure. A: The electron density pattern of H206A Orai. B: Viewing from the side, two facing subunits of H206A Orai are observed. C: The hexagonal arrangement is seen from the outer side of the cell. D: The entire structure is presented. The M1 helices are illustrated as blue ribbons, while the other helices are portrayed as cylinders (102).

1.8.The close conformation of Orai1 pore:

The arrangement of Orai and its activation process differs significantly from what's understood about other channels. To gain a better understanding of how STIM, a specific protein, triggers Orai's activity, examining their shapes using complete versions of these proteins will yield crucial insights at the molecular level (50).By employing X-ray technology, a detailed image of the resting Orai structure unveiled that the closed pathway is approximately 55 Å long, slender, and impermeable to ions (Figure 7B) (50). This structure comprises four segments: an outer circle formed by glutamate molecules that establish a filter (consisting of Glu178 components from the six segments), a hydrophobic part spanning around 15 Å, a basic part also extending about 15 Å, and an internal part within the cell (Figure 7B) (108). Changing the foundational unit corresponding to Glu178 in human Orai1 (Glu106) to aspartate disrupts the capacity to select calcium ions (108). The boundaries of the basic section are sculpted by three amino acids from each of the six M1 helices, which remain constant as lysine or arginine in Orai channels (Figure 7B) (47). Modifying the uppermost amino acid in human Orai1 (R91W, corresponding to K163W in Drosophila Orai) results in a severe immune deficiency-like condition by hindering channel activation (53). The presence of 18 fundamental units (three from each of the six segments) in the channel passage, forming a cation channel, is atypical and is likely responsible for creating a hindrance that prevents calcium ions from passing when the channel is closed (50).The closed structure of the basic section

serves as a location where anions can attach, providing stability to the neighboring arginine/lysine foundational units. Within this arrangement, something akin to an iron compound adheres to the channel, resembling a plug. While this may not be actual iron, it appears that this plug must shift to enable the passage of calcium ions when the channel is open(50).

Mutations within Orai that lead to enhanced activity offer a potential avenue to comprehend the structure of an open channel without relying on STIM to trigger it. Specific mutations in the M1 residues, which constitute the pathway of the channel, result in channels that remain consistently active. However, these channels don't display the same preference for allowing calcium ions as seen in STIM-activated Orai. This suggests that their pore shapes might differ from the natural configuration (92).Remarkably, the H134A mutation in human Orai1 doesn't contribute to the structure of the pore itself. Nonetheless, it produces an active channel that exhibits a marked preference for calcium ions, even in the absence of STIM (96). The strong selectivity of this mutant and its typical pattern of current response to changes in voltage suggest that this mutation triggers a pore configuration quite analogous to what transpires during the activation of Orai by STIM (94), (96).

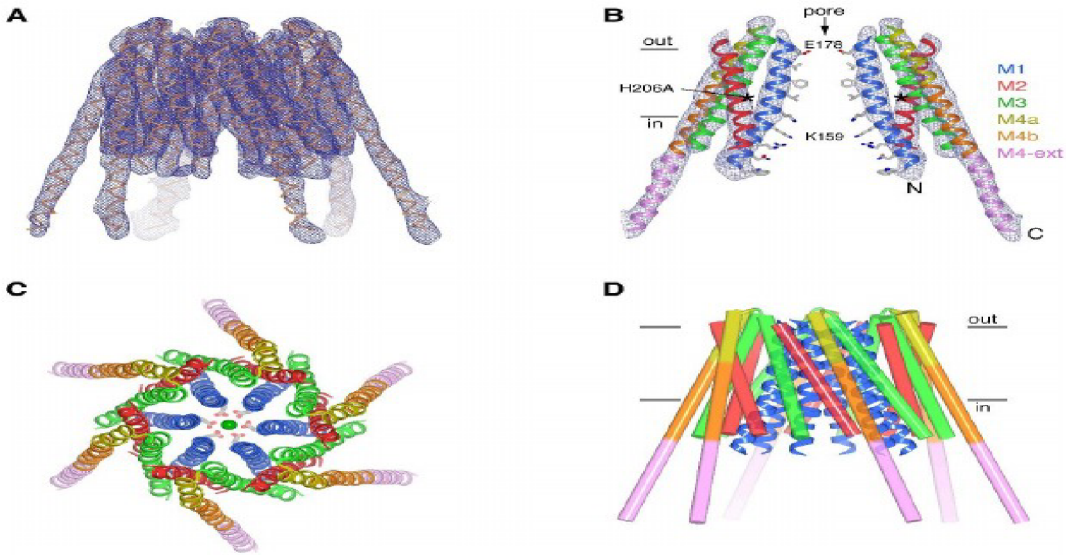

Figure 9 showcases the CRAC channel's hexameric structure through Orai1 subunit arrangement. In section A, a closed dOrai view displays a Ba2+ ion bound by glutamates and cytosolic M4 extensions. Section B presents two methods for constructing the hexameric channel using Orai1 concatemers. In section C, schematics depict glutamate side chains forming the Ca^{2+} filter in hexameric and tetrameric channel TM1 helices. Lastly, section D highlights the distinctive shapes and charges of these filters, leading to differing Ca^{2+} affinities.

2. Materials and Methods:

2.1. Plasmid DNA Purification:

To transfer specific DNA fragments into eukaryotic cells in the following step (transfection), it is crucial to isolate high-quality plasmid DNA. This can be accomplished by using a silica membrane column the size of an Eppendorf tube and by centrifugation. Additionally, proteins, RNA, and endotoxin contaminants are also eliminated in this step to ensure effective transfection (72,73).

To prepare the lysate, 600 µl of bacterial culture was mixed with 100 µl of cell lysis buffer by swirling the tube six times in a 1.5 ml microcentrifuge tube. Then, 350 µl of cold (4-8 °C) Neutralization solution was added and mixed by inverting the tube until the solution turned yellow. The supernatant (~900 µl) was then added to a mini column in a collection tube and centrifuged at maximum speed for 30 seconds. The flow through was discarded and the mini column was added to the same collection tube (73).

In the washing step, 200 µl of endotoxin removal solution (ERB) was added to the mini column and centrifuged at maximum speed for 30 seconds. Then, 400 µl of column wash solution (CWC) was added to the sample and centrifuged again at maximum speed for 30 seconds (72).

The mini column was transferred to a clean 1.5 ml microcentrifuge tube in the following elution step, and 55 µl of nuclease-free water was added directly to the mini column matrix. The sample was then incubated at room temperature for 1 minute and centrifuged for 30 seconds to release the plasmid DNA. 15 µl of the eluted plasmid DNA was put into a new tube for sequencing, while the remaining eluted plasmid DNA was stored at -20 °C (73).

To determine the DNA concentration, the measurement was taken using a nanodrop photometer through absorbance calculations. The DNA concentration of a nucleic acid is considered adequate if the curve produced corresponds to the typical curve for nucleic acids(74).

2.2. Transfection :

Transfection is the process of introducing foreign DNA into eukaryotic cells. The choice of cell line for this process is important, and in this case, human embryonic kidney cells 293 (HEK293) were chosen due to their ease of transfection and culture.

Lipofection is a specific type of transfection that involves binding the transfected DNA sequences to liposomes that surround them. The lipids surrounding the DNA carry a positive charge, which allows them to take up the negatively charged nucleic acids into the cell via endocytosis (75)(76).

To carry out the transfection, 15 µg of DNA was added to a sterile Eppendorf tube along with 10 µl

of transfection reagent (Transfectin). The DNA in this reagent is coated with lipids, which are recognized by the cells and taken up via endocytosis. The mixture was incubated at room temperature for 20 minutes and then drizzled onto HEK cell plates. The plates were then incubated at 37°C and 5% CO2 for 20-22 hours (77). Prior to transfection, 800 µl serum DMEM medium without additives was added to the tube (77).

2.3. Cell Lysis:

Cell lysis is a crucial step in protein extraction, where the proteins and lipids in the cells are solubilized. Various physical methods are available to achieve cell lysis, including mechanical disruption, liquid homogenization, sonication, freeze/thaw cycles, and manual disruption. The selection of a suitable method depends on the cell type, volume, and protein sensitivity. For this experiment, chemical and mechanical lysis methods were used.

To start, 1 mL of HBSS+1 mM EDTA mixture was used to pipette the 20-22h incubated HEK293 cells out of the dish and resuspended them a few times. The cell mixture was then transferred to an Eppendorf tube and centrifuged at 4600 rpm for one minute. The supernatant was discarded, and the pellet was resuspended again in the HBSS/EDTA buffer mixture. After another round of centrifugation, the supernatant was removed, and the pellet was resuspended in a mixture of 500 µL lysis buffer and 15 µL protease inhibitor. The Eppendorf tube was incubated on ice or in the freezer for 15 minutes (77)(78).

To mechanically disrupt the cell membranes, the incubated mixture was pulled through a 0.4 mm x 20 mm syringe multiple times and then centrifuged at 4600 rpm for 10 minutes. The supernatant was stored at -20°C, and the pellet residue was discarded. To further extract the proteins of interest, 20 µL of the supernatant was mixed with 5 µL of CuP solution, and the mixture was incubated for 5 minutes. The reaction was quenched by adding 5 µL of the quenching solution. The sample was then denatured by adding 10 µL of Laemmli buffer (sample buffer) and heating the solution at 55 °C for 10 minutes on a heating block(79)(80).

2.4. SDS-Page:

In SDS-PAGE, an electric field is used to transport charged molecules through a solvent. However, in this experiment, a gel of polymerized acrylamide monomers is used to separate biological molecules based on their net charge in an electric field. The pore size of the gel depends on the concentration of acrylamide, with smaller pore sizes required for the separation of low molecular weight proteins(81). To prepare the 12% polyacrylamide gel, 2.4 mL 30% acrylamide, 1.93 mL MilliQ water, 1.5 mL 1.5 M (pH 8.8) Tris, and 60 µL 10% SDS were mixed, and 90 µL 500 mg/mL APS and 3 µL TEMED were added rapidly. After approximately 30 minutes, a stacking gel

was formed by mixing 0.33 mL of 30% acrylamide, 1.5 mL of MilliQ water, 0.625 mL of 0.5 M (pH 6.8) Tris, and 25 µL of 10% SDS, and 15 µL of 500 mg/mL APS and 2.5 µL of TEMED were added quickly(82). The denatured and heated sample was centrifuged at high speed and mixed with loading dye, then pipetted into the wells of the polyacrylamide gel along with the protein standard. The SDS-PAGE was run at 150 V for approximately 1 hour and 15 minutes and stopped when the front of the loading dye hit the bottom of the gel(77).

2.5. Western Blot:

The SDS-page technique is commonly used to separate proteins by size in a polyacrylamide gel, and electrotransfer is used to transfer the separated proteins to a blotting membrane for detection. Electrotransfer involves applying an electric field perpendicular to the gel surface, with the blotting membrane placed between the gel surface and the anode. The proteins then migrate out of the gel and stain the membrane at the exact location of the protein bands in the gel (83)(84).

To perform electrotransfer, the stacking gel is removed, and the running gel is placed in transfer buffer along with a stack of filter papers. The blotting membrane is cut to match the shape of the gel, wetted with methanol, and then soaked in transfer buffer. A sponge is placed on a portion of the Western blot cassette, and a few sheets of soaked filter paper are placed on top. The gel is stacked on top of the papers, and the membrane is stacked on top of the gel. The cassette is sealed and placed in the holder filled with transfer buffer. The electrotransfer is typically performed for 1 hour and 30 minutes (82).

2.6. Electrotransformation:

To perform electrotransfer, a blotting sandwich was prepared. The cassette holder was filled with 1x blotting buffer, and a black sponge, a green sponge, a piece of filter paper, the polyacrylamide gel, a polyvinylidene fluoride (PVDF) membrane, another piece of filter paper, a green sponge, and a black sponge were arranged in the cassette holder and wetted with buffer. The gel was carefully removed from the gel cassette, and the edges of the cassette were tidied up to ensure good contact between the gel and the membrane.

2.7. Immunodetection:

Immunodetection is a powerful technique used to detect specific proteins of interest through the use of specific antibodies. The process involves blocking any non-specific antibody binding sites on the membrane using a blocking solution. Milk powder dissolved in TBST is a commonly used blocking agent due to its low cost, ease of preparation and storage compared to other reagents. The membrane is then incubated with a specific primary antibody that binds to the protein of interest, followed by a secondary antibody conjugated to an appropriate enzyme. The secondary antibody binds to the primary antibody, and the enzyme generates a signal for membrane imaging(83)(84).

To begin the immunodetection process, the membrane was carefully removed from the cassette using forceps and incubated in a blocking solution on a shaker for two hours. Subsequently, the membrane was washed with MilliQ water on the shaker for a few minutes to remove any excess blocking solution. The membrane was then immersed in a solution containing the primary antibodies, which in this case was rabbit anti-Orai1 antibody, and incubated on a shaker at 4°C for one hour. Following this, the membrane was washed three times with fresh TBST on the shaker for 10 minutes each. The membrane was then incubated in a secondary antibody solution containing HRP conjugated to rabbit antibody, and again shaken for one hour. Finally, the membrane was washed three more times with TBST on the shaker for 10 minutes each to remove any excess secondary antibody(84).

2.8. Chemiluminescence Detection:

To visualize the protein bands on the blot, the photographic paper is incubated in a dark room with red light and placed on top of the membrane in a hypercassette. Enzymes that are bound to the secondary antibody catalyze a reaction, producing a signal in the form of light that can be easily read. To trigger the chemiluminescence reaction, a mixture of 1 ml of luminol and 1 ml of hydrogen peroxide is infused over the membrane and the membrane is placed in the hypercassette.

To visualize the blot, the photographic paper is glued to the membrane in the hypercassette and incubated for approximately 30 minutes in a dark room equipped with red light. The transpiration of light through a film triggers the chemiluminescence reaction. After incubation, the photographic paper is immersed in the developer solution, fixer solution, or water, respectively. The protein bands become visible within a few seconds. (85).

2.9.PDB(Protein Data Bank):

The Protein Data Bank (PDB) is like a big library of information about the shapes of important molecules in our bodies. It focuses on proteins and nucleic acids, which are essential for life. Scientists use techniques like X-ray crystallography and NMR spectroscopy to figure out the exact 3D structures of these molecules(98).

The PDB was created in 1971 and has become a crucial tool for researchers studying the structure of biological molecules. It contains a huge collection of structures from many different organisms and molecules. Scientists from all over the world contribute to the PDB by sharing their own structures, which are then available to everyone through the database(98).

In this thesis, I utilized the Protein Data Bank (PDB) to access data related to three structures: the 4HKR Calcium release-activated calcium (CRAC) channel ORAI, the 4HKS Calcium release-activated calcium (CRAC) channel ORAI with the K163W mutant, and the 6BBF structure representing the CRAC channel Orai in an open conformation with the H206A gain-of-function mutation. These structures were chosen from the fruit fly species Drosophila melanogaster, as they provide an easily evaluated and comparable model to the human counterpart.

By accessing the PDB files of these three structures, I utilized PyMOL to conduct detailed evaluations and explore the differences between the closed and open channels. This allowed for a more comprehensive understanding of the structural variations and functional implications of these channels.

2.10. PyMOL:

PyMOL is a widely recognized and widely used molecular visualization software in the field of structural biology. It allows researchers to interactively visualize and analyze three-dimensional molecular structures, including the ability to load structures from the Protein Data Bank (PDB). PyMOL offers a range of customizable options for interpreting and representing structures, and it provides useful tools for analyzing distances, angles, docking simulations, and protein-ligand interactions. The software supports Python scripting, enabling users to customize and automate tasks and integrate with other tools and databases. PyMOL is known for its versatility, user-friendliness, and its value in various scientific disciplines, particularly in biochemistry and drug discovery, where it facilitates effective visualization and analysis of structural information.

3. Results and discussion

3.1. Task:

The Drosophila melanogaster Orai channel, known as dOrai, presents itself as a hexameric protein consisting of six subunits, each featuring four transmembrane (TM) helices(50). The crystallization process of the dOrai channel played a pivotal role in unraveling insights regarding its compositional arrangement, subunit interplay, and extrapolating findings to the human Orai channel(101). Within this context, TM1 serves as the foundational pore-forming element, encircled by additional TM domains in a tranquil state. This structural configuration ensures the channel's steadfastness and stability(50).

Hou et al demonstrated that the cytosolic regions of the open pore experienced considerable expansion compared to the closed pore. Further x-ray crystallography investigations unveiled an unlatched-closed configuration that resembled a combination of the quiescent and open states. Regarding the Orai channel's three conformations, they put forth a theoretical sequence for channel activation. This sequence suggests that, upon STIM1 binding, the initially closed pore state transitions, via an unlatched-closed conformation, to an open pore state(109).

Long et al. utilized the H134A Orai1 mutation with gain-of-function properties to facilitate the crystallization of the active dOrai channel(109). The resulting crystal structure indicates alterations in conformation and the alignment of both TM4 and the elongated TM4 region (M4ext) during the process of channel activation(50).

Frischauf et al demonstrated that the introduction of the H134A mutation into TM2 of human Orai1 creates an active channel that closely resembles the conformation of naturally occurring open channels (101). Subsequently, the crystal structure analysis of the H206A mutation in dOrai (equivalent to H134A in human Orai1) revealed that the overall structure of the open channel is similar to the quiescent conformation. This structure forms a six-part arrangement of Orai1 building blocks. The findings provide valuable insights into the intricate dynamics of channel activation and conformational changes(101).

In this bachelor's thesis, we aim at investigating the structure of cancer-associated mutants of Orai proteins. Furthermore, different methods shall be compared. The first method used is bioinformatic prediction with the use of PYMOL to see whether mutants from cbioportal.org are able to change the structure of specific amino acid side chains and if the distance to other side chains is altered.

To perform measurements using PyMOL, the structures utilized from the Protein Data Bank (PDB) are specific to Drosophila Orai. The structures employed include 4HKR and 4HKS, which represent the closed channel state, and 6BBF, which represents the open channel state.

The objective is to compare Drosophila Orai with human Orai. In Drosophila Orai, a mutation of K163W is used, which is equivalent to the R91W mutation in human Orai(101).
For the human counterpart, the references used involve evaluating t0he closed channel state with the R91C mutation in Orai, as well as the open channel state with the R91C+H134A mutation.
The H134A mutation in human Orai1 not only induces channel opening but also maintains nearly normal Ca^{2+} selectivity, even in the absence of STIM1 (109)(110). A comparative analysis between the H206A (6BBF pdb) structure of the analogous dOrai and the closed WT dOrai structure reveals two significant modifications. Firstly, the M4ext helices are extended, breaking free from their previous paired coiled-coil interactions. Secondly, the inner pore of the H206A channel experiences substantial dilation (approximately 10 Å), attributed to a rigid rotation of all four TM helices away from the pore axis. This rotation effectively removes a conduction obstacle that had previously been caused by anion binding among the three rings of closely positioned basic residues in the closed state. Notably, the detection of iodide within the open pore structure implies that intracellular anions could potentially aid the passage of Ca^{2+} through this region by counterbalancing the positive charges lining the inner pore(101).
An additional configuration in the closed state, characterized by straightened M4 extensions, has provided evidence that merely disrupting the coiled-coil arrangement of M4ext is inadequate to initiate channel opening(109). Nevertheless, this disruption plays a pivotal role in establishing sufficient room for the outward motion of the TM helices, an essential requirement for transitioning to the open state. According to the proposal by Hou et al(109), the interwoven M4ext helices function akin to latches, contributing to the stabilization of the closed state by facilitating interactions between M4 and M3. These latches need to be released before STIM1 can bind and initiate the process of channel opening(109).An alternative gating model, rooted in molecular dynamics simulations and cysteine crosslinking experiments involving the H134A Orai1 mutant, suggests a more measured enlargement of both the hydrophobic and basic portions within the pore. Furthermore, this model postulates a rotation of R91 side chains towards the perimeter of the pore(96).

Scientists are interested in understanding the structure of a protein called Orai when its pore is open(97). However, studying the interaction between Orai and another protein called STIM presents challenges due to their weak interaction and the unknown ratio between them(97).To address this issue, researchers have investigated mutations in Orai that lead to a constantly active channel, meaning it remains open without the involvement of STIM(96). However, these mutated channels have shown reduced specificity for calcium compared to the Orai channels activated by STIM,

indicating differences in the shape of their pores.One specific mutation, H134A in human Orai1, has been identified as activating the channel with a high degree of calcium selectivity even in the absence of STIM(97). This mutation induces a pore conformation similar to that observed when Orai is activated by STIM(96).In this study, aimed to introduce a similar mutation, H206A, into Drosophila Orai, and confirm its ability to generate a constantly active channel. They utilized data from the Protein Data Bank (PDB) and analyzed the channel structure with the H206A mutation in Drosophila, which is equivalent to the R91W mutation in humans(97). The resulting structure revealed a wider pore, and certain regions underwent conformational changes necessary for pore opening(96).

The objective of this thesis is to investigate the structure of the Calcium Release-Activated Calcium (CRAC) channel ORAI in relation to Drosophila melanogaster using the PDB database. Two structures, 4HKR and 4HKS, were utilized from the PDB to examine a basic region near the intracellular side that can bind anions, potentially stabilizing the closed state of the channel. The unique architecture of the ORAI channel, distinct from other ion channels, provides insights into the principles of selective calcium permeation and gating.

Additionally, the third structure, 6BBF, represents the CRAC channel ORAI in an open conformation. The H206A gain-of-function mutation was applied to this structure, obtained from the PDB database.

The first step of this thesis involved visualizing the structures from the PDB (4HKR(wild type) and 4HKS (K163W mutant), and 6BBF(Open channel)) in PyMOL. The PDB file of 4HKR was compared with 6BBF to compute the distance between the open and closed channel conformations. The same comparison was performed between 4HKS and 6BBF.

The second step focused on comparing the Drosophila ORAI structures with human ORAI. For this comparison, references were used to evaluate immunodetection results. Specifically, the R91C mutation in human ORAI was considered equivalent to the K163 mutation in Drosophila. Furthermore, the R91C+H134A mutation was examined as an open channel state, comparable to the 6BBF structure of Drosophila melanogaster.

In conclusion, the results obtained from both the PyMOL computations and immunodetection of human ORAI were compared with the data related to Drosophila. This comparison aimed to identify any differences and provide insights into the structural characteristics of ORAI in these organisms.

3.1.1.The structure of 4HKR in the Protein Data Bank (PDB):

The protein 4HKR, known as Orai in Drosophila melanogaster, is crucial for forming the calcium release-activated calcium (CRAC) channel on the cell membrane. When calcium levels in the endoplasmic reticulum decrease, Orai is activated, leading to sustained calcium signals within the cell. By studying the crystal structure of Orai from Drosophila melanogaster, we have gained valuable insights(95).The calcium channel consists of six Orai subunits arranged in a hexagonal pattern, creating a central pore that extends from the cell membrane into the cytosol. A ring of glutamate residues on the extracellular side acts as a selective filter, allowing specific ions, like calcium, to pass through. On the intracellular side, a region with basic amino acid residues can bind to anions, potentially stabilizing the closed state of the channel(95).The architecture of the Orai channel is distinct from other ion channels, demonstrating unique characteristics and mechanisms that control the selective permeation of calcium ions and the opening and closing of the channel (gating)(97).

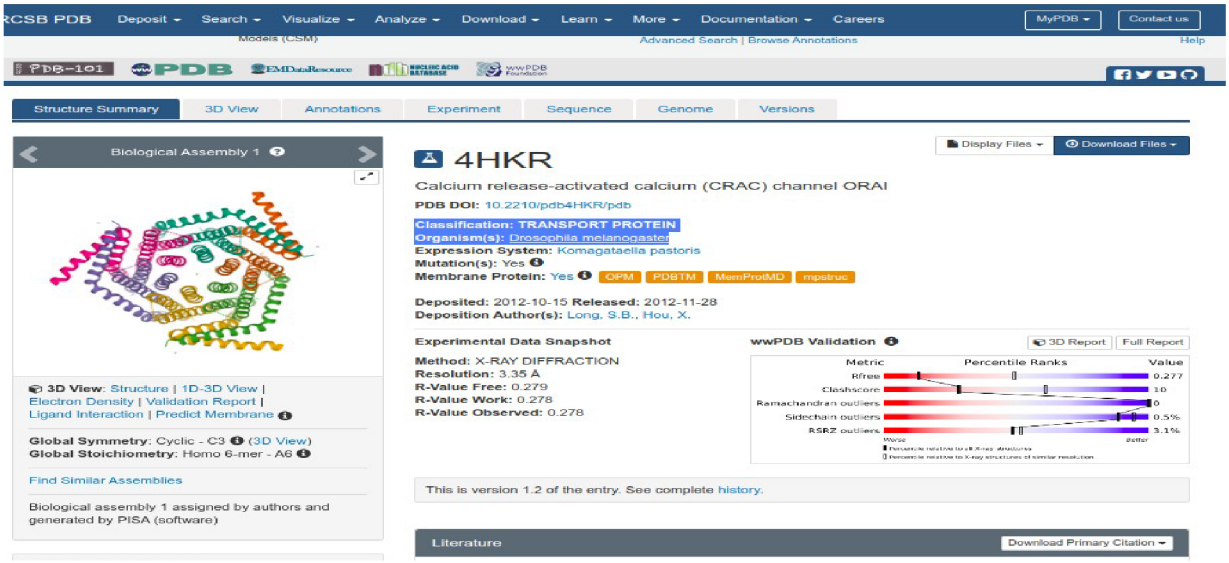

Figure 10 : PDB entry of 4HKR

3.1.2.The structure of 4HKS in the Protein Data Bank (PDB):

The protein 4HKS is a mutant form of the CRAC channel ORAI found in Drosophila melanogaster, specifically with the K163W mutation, which is equivalent to the R91W mutation in human Orai1(101). ORAI is a protein located on the cell membrane and plays a crucial role in generating sustained calcium signals when calcium levels are low in the endoplasmic reticulum(100).

By studying the crystal structure of ORAI from Drosophila melanogaster at a resolution of 3.35 angstroms, scientists have discovered important characteristics of the calcium channel. It is

composed of six ORAI subunits arranged in a hexagonal pattern, forming a central pore that extends from the cell membrane into the cytosol(50). The extracellular side of the pore has a ring of glutamate residues acting as a selective filter for calcium ions. Near the intracellular side, there is a basic region that can bind to anions, potentially stabilizing the closed state of the channel(100).

Compared to other ion channels, the architecture of ORAI is unique and provides insights into selective calcium permeation and channel gating mechanisms. These findings significantly contribute to our understanding of how cells regulate calcium levels(100).

In comparison to 4HKR, which represents the wild-type form of the protein, 4HKS carries the K163 mutation(95).

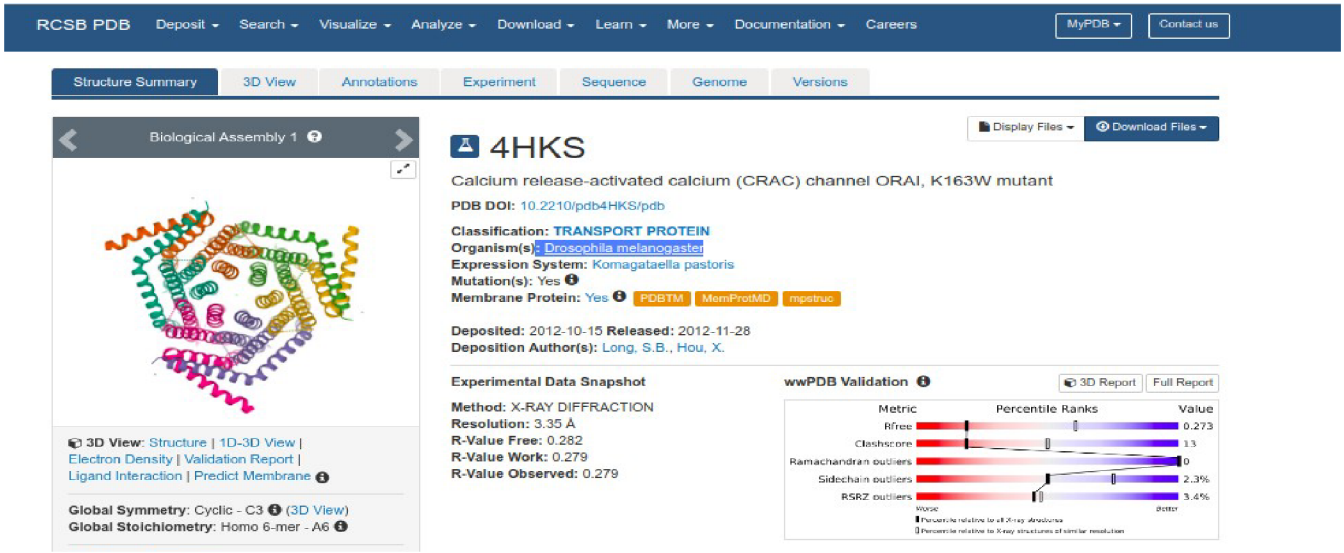

Figure 11: PDB entry of 4KHS

3.1.3.The structure of 6BBF in the Protein Data Bank (PDB):

The Protein Data Bank (PDB) entry 6BBF provides valuable structural information about the CRAC channel Orai in an open conformation. This structure was determined using cryogenic electron microscopy (cryo-EM) techniques. Additionally, the 6BBF entry includes the H206A gain-of-function mutation, which is of particular interest in understanding the channel's functionality.

To conduct a comprehensive comparison of the conformational transition between the closed and open states, we have specifically selected the mutant H206A structure (PDB: 6BBF) as the primary representation of the open state in this thesis. Conversely, the closed state is represented by the wild type structure (PDB: 4HKR), which has been deemed a suitable representative(103). These deliberate choices enable us to effectively examine and contrast the dynamics between the two states, contributing to a thorough analysis.

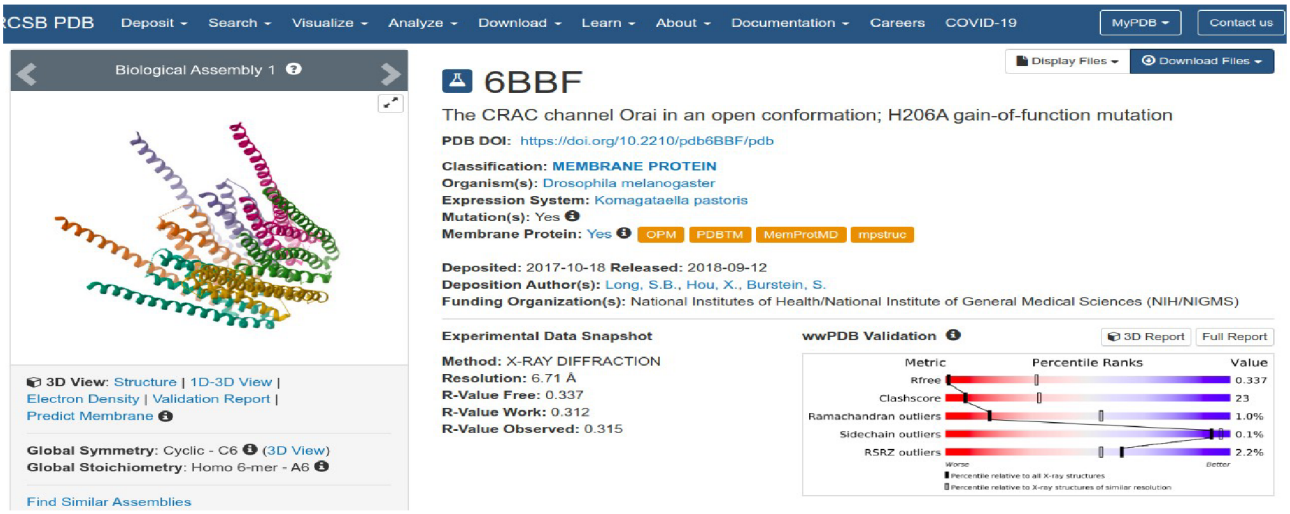

Figure 12: PDB entry of 6BBF

The structures 4HKR and 6BBF are compared, representing the closed and open channels, respectively(104). In 4HKR, there is a pore and a double-bent TM4 helix divided into three segments: TM4a on the extracellular side, central TM4b, and TM4-ext helix on the cytosolic side. The TM4-ext helices of neighboring subunits form a coiled-coil structure, believed to be where the STIM1 activator docks(105).

In contrast, the 6BBF structure features a wide pore and fully extended TM4 helices(104). The classification of 4HKR as the closed state contradicts experimental calcium flow measurements, as the pore radius is large enough to accommodate water molecules or dehydrated calcium ions. The occlusion and permeability characteristics of the pore suggest a hydrophobic gating mechanism similar to evaporation in nanoconfinement, where the formation of a vapor bubble stops the flow of liquid water and ions. The hydrophobic region of the pore appears well-suited for this mechanism(104).

3.2.PYMOL:

In this project I used PyMol which is one of the most widely used bioinformatics software. Commonly it is used as a molecular viewer to visualize macromolecules and small molecules. In this thesis I make use of this software for investigating Orai1 mutations, thereby comparing pdb data of 4HKR and 4HKS and 6BBF.In the PyMOL software open the data file related to the 4HKR. The following image represents the structure of 4HKR in PyMOL.

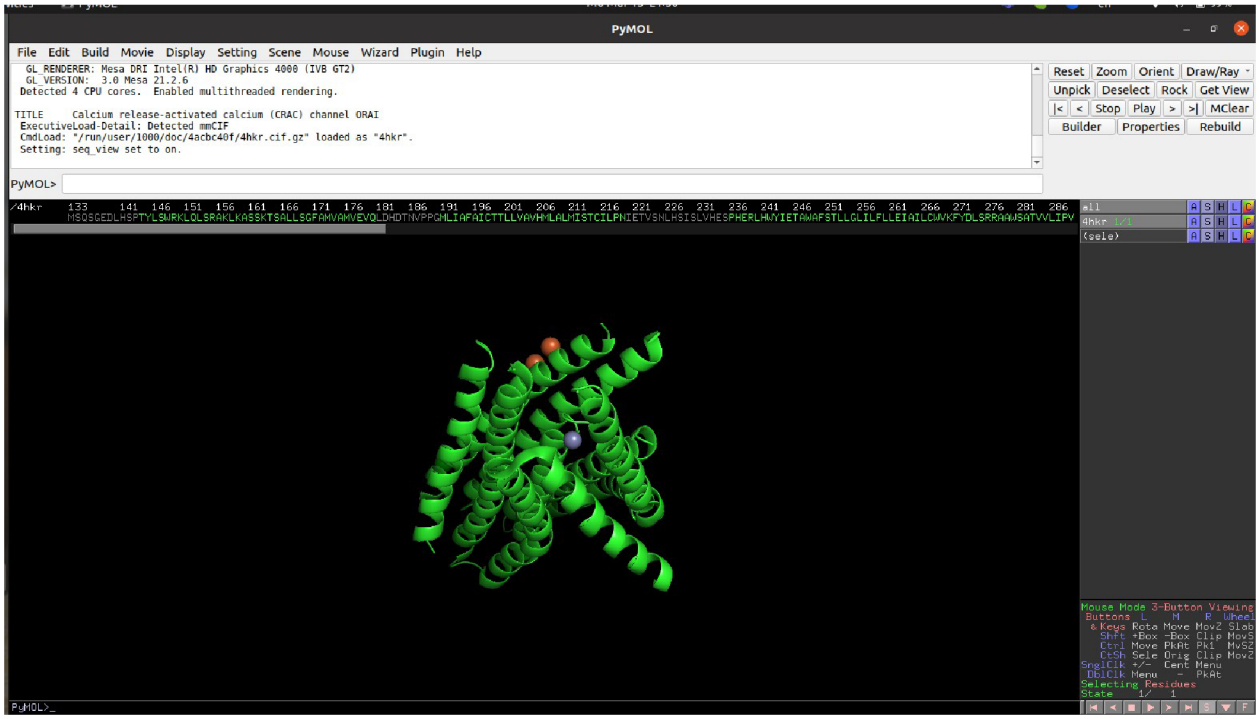

Figure 13: Image of proteins from 4HKR with turn on the sequence

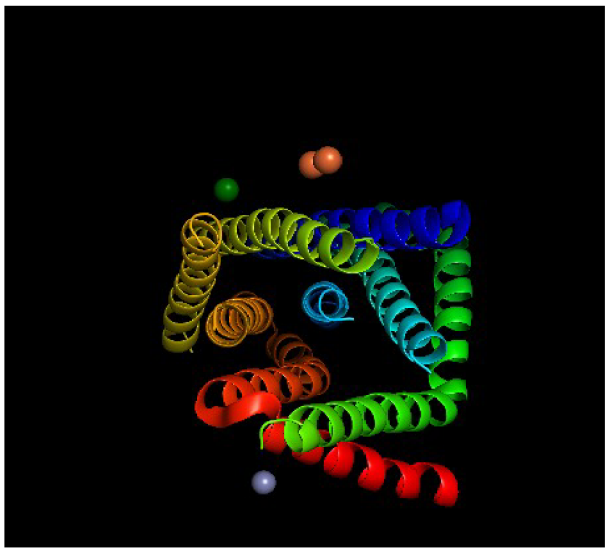

Figure 14 : Colored chain of protein by spectrum

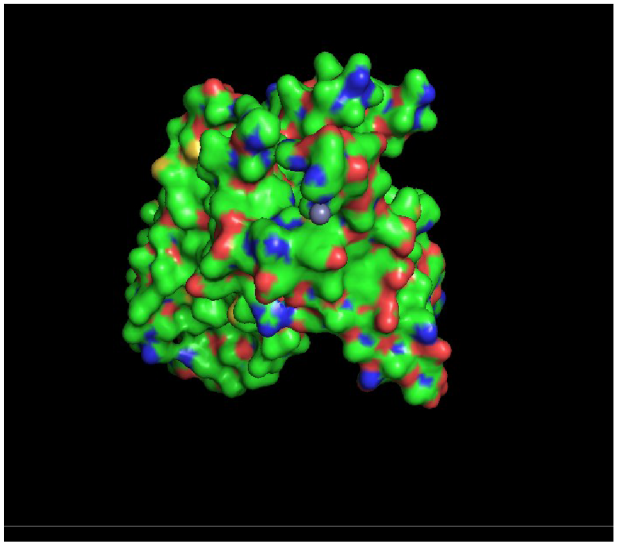

Figure 15: Surface of the 4HKR

To generate the cemetery maze, first select the "Action" tool and choose the "Generate" option. Then, select four different actions to create the maze layout(116). In the toolbar menu, you will find a range of new objects that you can use to customize the maze and enhance its overall appearance. Once you have added all the necessary objects, you should be able to see a clear picture of the maze. In Figure 16, you can see the maze with four dimers added to create the desired effect.

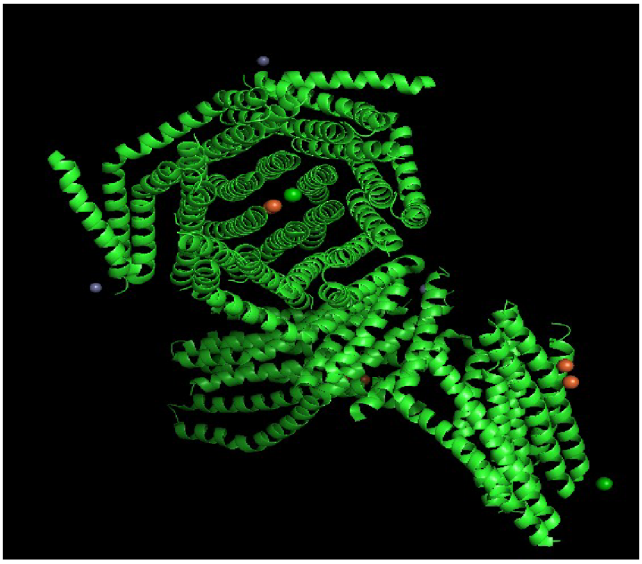

Figure 16 : Adding 4 different dimers in 4HKR

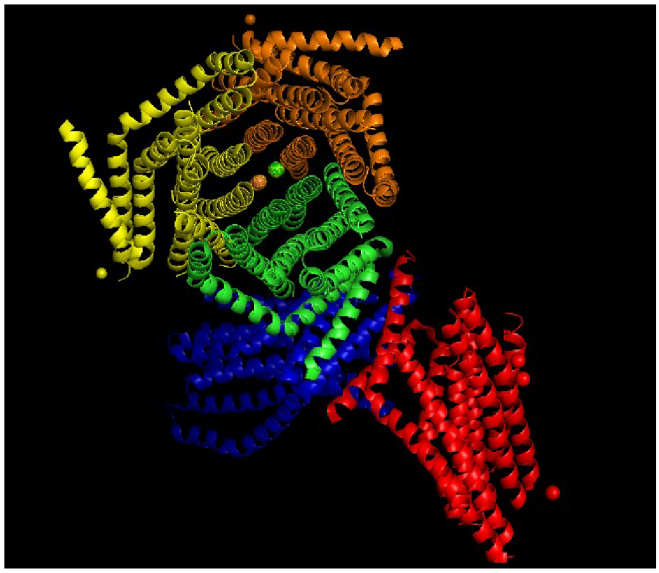

Figure 17: 4 added symmetry maze in 4 different color 4HKR is green here

For further comparison, I also referred to the PDB image and observed that the third section, which I represented in orange color, along with the first symmetry maze that I represented in yellow color, exhibited greater similarity to the PDB picture. This finding reinforces the conclusion that the symmetry sections one and three are the most informative for illustrating the symmetry and relationships between the dimers, as displayed in 4hkr.

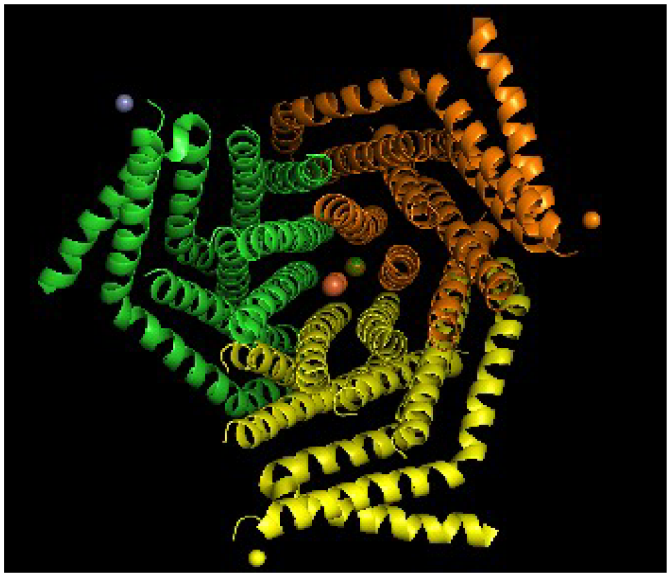

Figure18: First (yellow)and 3rd dimeres (orange)with 4hkr

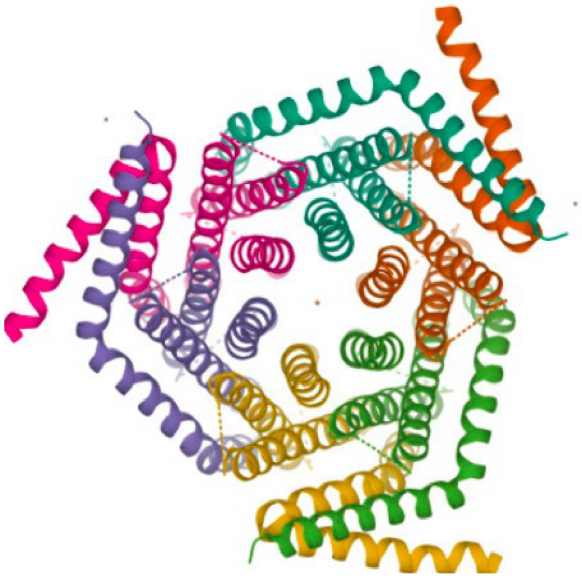

Figure19:PDB photo of 4HKR

In PyMOL, the term "symmetry maze" refers to a feature that helps visualize and explore the symmetry-related units in a crystal structure. Crystal structures often contain repeating units called asymmetric units, which are transformed by symmetry operations to generate the complete structure. The symmetry maze in PyMOL helps navigate through these symmetry-related units.

The usage of the symmetry maze in PyMOL allows you to visualize and analyze the relationships between the asymmetric units and the complete structure. It provides a graphical representation of how the asymmetric units are transformed and arranged within the crystal lattice(116). This feature can be particularly useful when studying crystallographic symmetry and understanding the packing of molecules in a crystal.By using the symmetry maze in PyMOL, you can gain insights into the symmetry operations and spatial relationships within the crystal structure, aiding in the interpretation and analysis of the structural data(Figure 18,Figure 19).

After selecting the first and 3rd group, which is the symmetry group, I copied it and added it to 4HKR. To visualize the resulting structure, I used the "color by chain" tool in the toolbar. The resulting figure shows four distinct molecules, as illustrated in Figure 18.

3.3. Comparative Analysis of Distance Measurements:

3.3.1 Closed Channel 4HKR and Open Channel 6BBF:

To gain a more detailed understanding and make a better comparison between the open and closed channel structures in PyMOL, I represented the closed channel structure, 4HKR, and the open channel structure, 6BBF. Using specific command lines, I measured the distance between residue K163 (which corresponds to R91 in humans) in both 4HKR and 6BBF. The calculated distance between these two residues in the structures is 58.5 angstroms (Figure 20).

Figure 21 assesses the similarity between the closed channel structure 4HKR and the open channel structure 6BBF through structural alignment. The alignment results are visually represented in Figure 21, with the blue structure corresponding to 4HKR and the red structure corresponding to 6BBF.

Structural alignment was performed using the "align" command in PyMOL. The objective was to superimpose the two protein structures to explore their degree of resemblance.

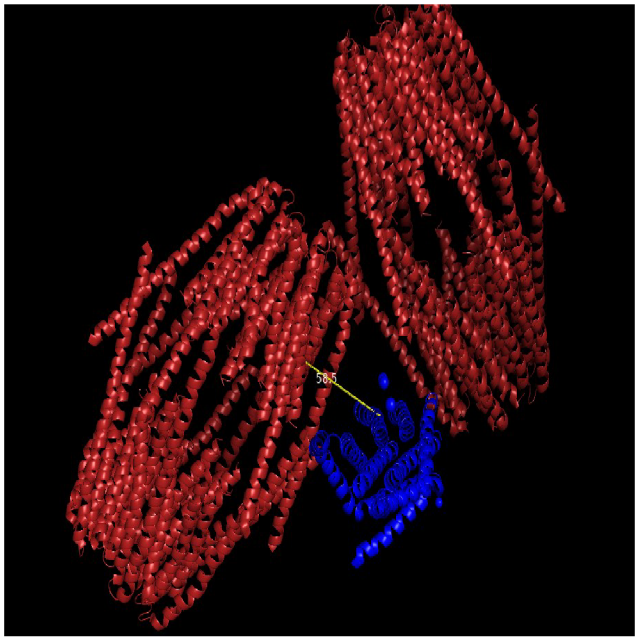

Figure 20 : The measured distance is between residue K163 in the closed channel 4HKR (depicted in blue) and the open channel 6BBF (depicted in red).

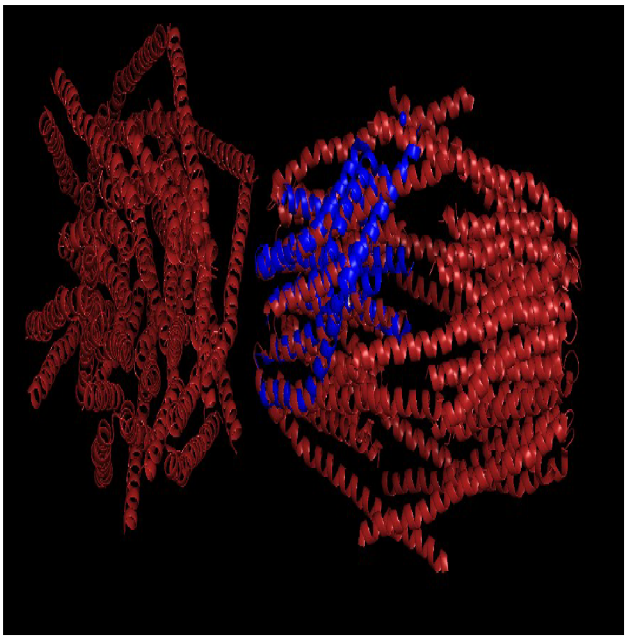

Figure 21: Structural Comparison of Closed Channel 4HKR (Blue) and Open Channel 6BBF (Red) with alignment

After alignment, the overall Root Mean Square Deviation (RMSD) between the two structures was calculated to be 1.951 Å, based on 1605 aligned atoms.

The structural alignment of 4HKR and 6BBF demonstrated a noteworthy similarity between the two channel structures. The high number of aligned residues (432 vs. 5136) and a substantial MatchAlign score of 2152.000 indicate a close resemblance. The rejection of a limited number of atoms during the alignment cycles may be attributed to local structural variations or flexible regions.

The results from the structural comparison of closed channel 4HKR and open channel 6BBF provide valuable insights into their degree of similarity. The alignment of the two structures with a low RMSD value of 1.951 Å supports the notion that they share substantial structural homology. This analysis contributes to a better understanding of their conformational relationships and potential functional implications.

3.3.2. Closed Channel 4HKS and Open Channel 6BBF:

After comparing the closed and open structures between 4HKR and 6BBF, I proceeded with the alignment and distance measurements for two CRAC channels: 4HKS , and 6BBF..In comparison to 4HKR, which represents the wild-type form of the protein, 4HKS carries the K163

mutation. This comparative analysis provided valuable insights into their conformational variances and potential functional implications.

My primary focus was on residue K163 in both channels, allowing me to thoroughly examine the variations in distance between them. This analysis revealed the distinct structural states of the closed channel (4HKS) and the open channel (6BBF), with a measured distance of 58.3 angstroms, as depicted in (Figure 22).

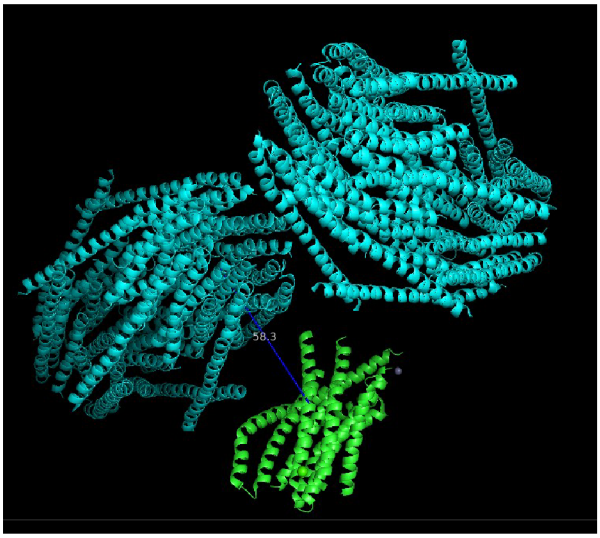

Figure 22:The measured distance is between residue K163 in the closed channel 4HKS(depicted in green) and the open channel 6BBF (depicted in blue).

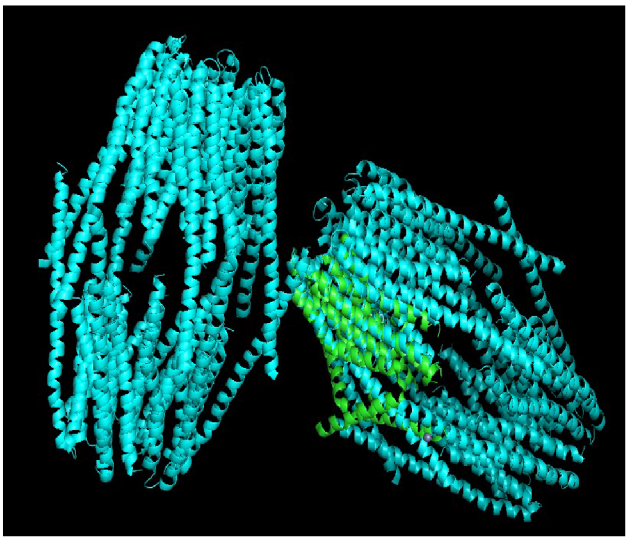

Figure 23: Structural Comparison of Closed Channel 4HKS (green) and Open Channel 6BBF (blue)

In Figure 23 it present the alignment and scoring results of the 4HKS and 6BBF structures. The alignment process, according to the PYMOL in the command line, paired 430 residues from 4HKS with 5136 residues from 6BBF, resulting in a total of 430 x 5136 pairwise scores to assess their structural similarity.

Using MatchAlign, we performed the alignment and successfully aligned a total of 2298 atoms between the two structures. Throughout the alignment process, certain atoms were rejected in several cycles due to their deviations from the aligned conformation.

The final Root Mean Square Deviation (RMSD) value of the aligned atoms was calculated to be 1.959 Å, based on 1599 aligned atoms. This RMSD value indicates a close structural resemblance between the closed channel structure (4HKS) and the open channel structure (6BBF), with only minor deviations observed during the alignment cycles.

The structural alignment and scoring matrix revealed a significant similarity between 4HKS and 6BBF, providing valuable insights into their conformational relationships and functional implications. This analysis enhances our understanding of these structures and their potential significance in their biological context.

3.3.3. A Comparative Analysis of Closed Channel and Open Channel Structures:

Through direct alignment, the closed channel 4HKR and open channel 6BBF exhibit a remarkable structural resemblance. The alignment process successfully aligned 1605 atoms with a final Root Mean Square Deviation (RMSD) value of 1.951 Å, highlighting the close similarity between these two structures. Despite minor variations observed with the rejection of a limited number of atoms during alignment cycles, the overall alignment emphasizes the substantial similarity between 4HKR and 6BBF.

Additionally, utilizing a scoring matrix to compare 4HKS and 6BBF reveals a significant similarity between these channel structures. The MatchAlign score of 2136.000 and the final RMSD value of 1.959 Å further confirm their structural resemblance. The alignment process aligned 430 residues from 4HKS to 5136 residues of 6BBF, totaling 2298 aligned atoms. Although some atoms were rejected during alignment, the overall structural similarity remains evident, providing valuable insights into their conformational relationships.

Both comparative analyses demonstrate a notable structural similarity between the closed channels (4HKR and 4HKS) and the open channel (6BBF). These alignments shed light on the conformational relationships and potential functional implications of these channel structures. The findings enhance our understanding of channel gating and functionality regulation, offering valuable information for future investigations in the field of structural biology.

3.4. constitutively-active Orai1-H134A mutant in comparison to the wild-type Orai1:

The Orai1-H134A mutant has a larger pore size in a specific region compared to the wild-type Orai1(96). To investigate the mechanism behind this mutation's effect on the channel, the researchers examined the structure of both the wild-type and mutant Orai1 channels in a lipid bilayer using molecular dynamics simulations(101). Two gating sites in the pore were identified, one formed by hydrophobic amino acids and the other by basic amino acids(91). The simulations

showed that the Arg91 amino acid in the basic gate segment functions as a gate, and mutations in this region can affect the channel's permeability to calcium ions(96). The Orai1-H134A mutant exhibited increased flexibility in this region, resulting in a slightly wider pore compared to the wild-type Orai1, while still maintaining calcium selectivity(101). This mutation's effect on the pore size was not as great as other mutations that completely blocked calcium permeation(101).

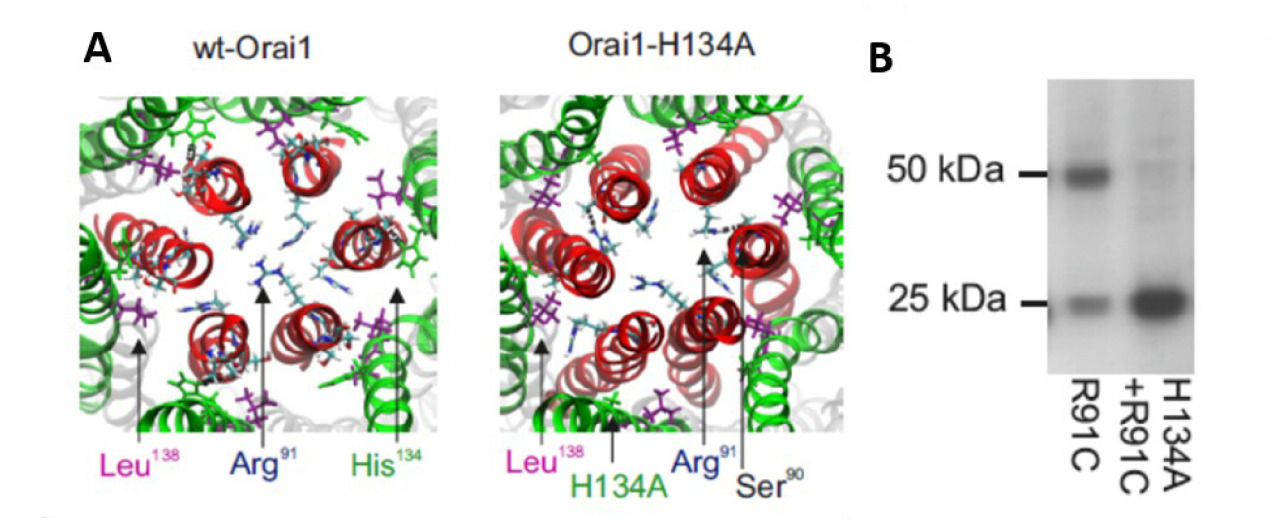

Figure 24 :(A):Top-down view of the wild-type Orai1 pore as depicted in molecular dynamics simulations. It highlights the side-chains of Arg91, His134, and Leu138.And molecular dynamics simulations of Orai1-H134A. (B):Chemiluminescence Detection of the Membranes H134A+R91C(101)

3.4.1. Chemiluminescence Detection of the Membranes H134A+R91C VS to R91C:

Frischauf et al. employed a systematic approach involving cysteine scanning to compare the pores of the wild-type Orai1 and Orai1-H134A channels(103). They introduced individual cysteine replacements along the pore-forming TM1 helix (Arg83 to Glu106) of Orai1 and Orai1-H134A, both of which lacked inherent cysteines(111),(112). This enabled them to assess dimerization levels. When Cu2+-phenanthroline was introduced to facilitate cysteine crosslinking, the cysteine-free versions of Orai1 and Orai1-H134A remained as individual units. However, with single cysteine substitutions, a combination of monomeric and dimeric bands appeared, contingent upon the specific location within the channel (depicted in Fig25. E-G)(101).Their investigation revealed that the most prominent level of dimerization among the Orai1 residues forming the channel pore was observed at specific positions: Glu106, Val105, Val102, Leu95, Arg91, and Ser90. These positions were interspersed with stretches of residues that exhibited lower levels of reactive cysteine

crosslinking, as depicted in Figure 28F. These findings align with the positioning of these residues facing the pore, which is consistent with outcomes from our Orai1 molecular dynamics simulations, the crystalline structure of the dOrai pore, and prior research (86)(112)(92).
As depicted in Figure 28F, a thorough analysis of the atomic structure of dOrai (86) provided valuable insights, leading to the identification of Phe99 as an additional point of constriction. This discovery gains further support from findings in previous research and their utilization of cysteine scanning techniques, suggesting that Gly98 is positioned in closer proximity to the central region of the pore (92, 112).

In the subsequent step, using a comparable cysteine scanning strategy, they determined the configuration of the channel in the Orai1-H134A mutant, which remains in a constitutively active state. Similar to the wild-type Orai1, effective crosslinking involving cysteines was observed in the vicinity of the selectivity filter, including Leu95. The decrease in crosslinking efficiency, similar to the outcomes from their molecular dynamics simulations (illustrated in Figure 25D), is likely due to the decreased flexibility of these cysteine side chains(101).
The middle segment of the Orai1-H134A pore, spanning from Phe99 to Ser93, exhibited an overall increase in crosslinking levels. This augmentation was especially notable for F99C, G98C, A94C, and S93C (as demonstrated in Figure 25G)(86). These findings corresponded with the heightened flexibility detected within the open pore, as observed in their molecular dynamics simulations (as shown in Figure 25D)(101).

The most notable distinction in crosslinking patterns was observed with R91C and F99C. While R91C demonstrated crosslinking in the wild-type Orai1, such interaction was absent in the Orai1-H134A mutant (depicted in Figure 25E-G)(101).

The outcomes of molecular dynamics simulations on Orai1-H134A also revealed an expanded pore size at Arg91 (depicted in Figure 25B) and an increased separation between side chains, as observed when compared to the wild-type Orai1 (as demonstrated in Figure 25B). Overall, these findings imply that both wild-type Orai1 and Orai1-H134A share similar pore characteristics, undergoing two localized yet crucial conformational changes: an enlargement of pore dimensions within the hydrophobic segment and the region surrounding Arg91. These subtle adjustments during the gating of Orai1 are expected to uphold specific structural constraints within the pore, thereby offering an explanation for the remarkably low femto Siemens (fS) conductance of Ca^{2+} ions through Orai1 (101).

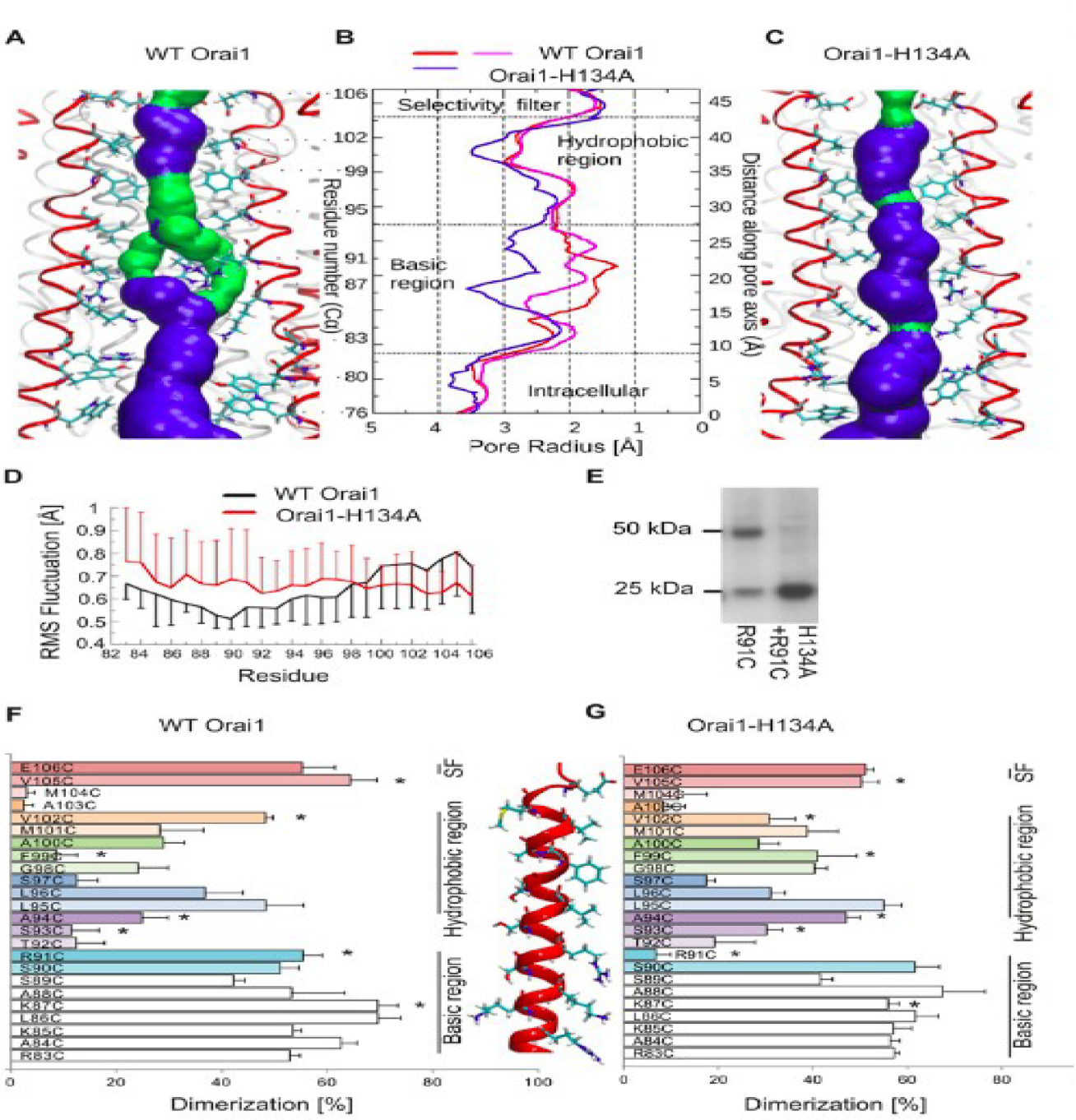

Figure 25:Enlarged pore dimensions observed in the open state of Orai1-H134A channels

(A-C) dynamics simulations comparing wild-type Orai1 and Orai1-H134A channels. (A)Snapshots show the channel's TM1 helices and pore lining residues. (C)Pore surfaces are color-coded. Average pore radius differences are plotted for both channels.(G) Fluctuations of individual TM1 residues are measured. (E)Crosslinking experiments demonstrate monomer-dimer formations. (F,G)Dimerization efficiency (%) from cysteine crosslinking is assessed for engineered cysteines in TM1 pore segments of both channels. (F)Parallel experiments with significant differences ($p < 0.05$) are indicated(101).

3.4.2.K163W mutant:

In this thesis, I utilized the 4HKS pdb entry linked to Drosophila, which features the K163W mutant.The crystal structure of the K163W mutant provides insight into the fundamental region of the pore. Despite the mutant closely resembling the wild-type (WT) pore in its overall structure, exhibiting only a marginal difference at the present resolution (with a root mean square deviation of 0.1 Å for Cα atoms), a distinct alteration is evident: the tryptophan residue at position 163 extends into the pore(Figure 26C). This modification leads to a densely packed arrangement of six tryptophan residues—one from each subunit—thereby elongating the hydrophobic segment of the pore by an extra helical turn(86),(50).

Remarkably, the electron-density maps of the K163W mutant reveal a surprising absence of the anticipated anomalous-difference density linked to iron within the pore. This finding aligns with the results obtained from inductively coupled plasma mass spectrometry (ICP-MS), which indicate a reduced iron content in the K163W mutant protein compared to the wild-type. Additionally, the mutant exhibits less distinct electron density for Lys159 and Arg155, likely attributable to the absence of an anion (as depicted in Figure 26D)(86).

To investigate the effect of the K163W mutant on anion binding, an anomalous-difference electron-density map was generated by soaking a crystal in (IrCl6)3-. Interestingly, the distribution of the anion within the pore differs from that of the wild-type pore. Specifically, a single peak (12σ) is observed in the K163W mutant pore, located between Lys159 and Arg155, indicating the elimination of one anion binding site (Figure 26C)(95)(50).

An analogous dOrai structure in Drosophila, encompassing the K163W mutation equivalent to the human Orai1 mutation R91W, reveals altered anionic interactions within the core region. This observation bolsters the notion that channel gating is influenced by the fundamental region, underscoring the possibility that an unidentified physiological anionic element, like phosphate, might play a role in sustaining the channel's closed state (113).

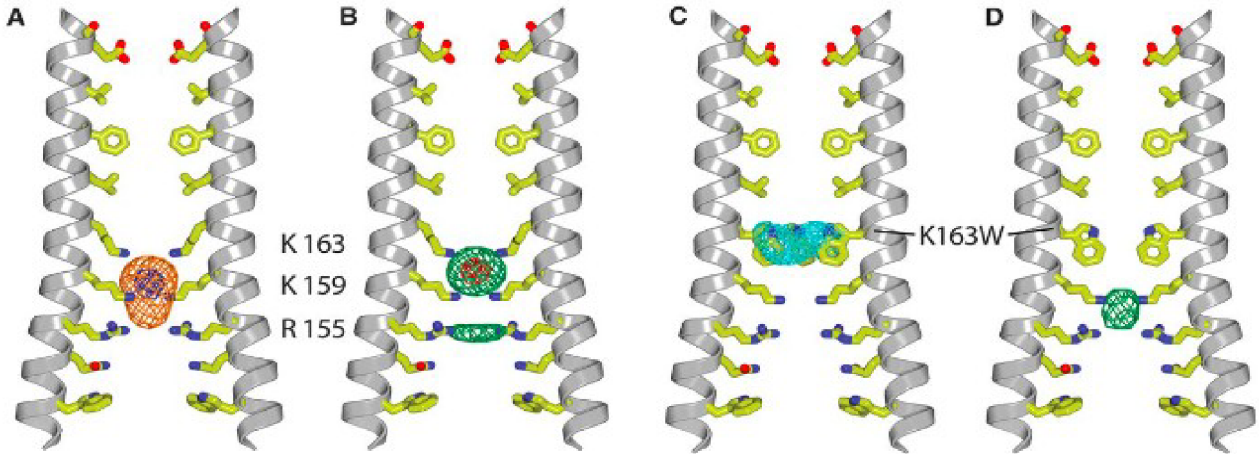

Figure 26:The graph displays electron density maps and anomalous-difference density in the context of anion binding and the K163W mutant. In Figure (A), the maps illustrate the basic region of the WT pore derived from unsoaked crystal data. Figure (B) highlights anomalous-difference density in the WT pore with (IrCl6)3– soaking. Figures (C) and (D) focus on the K163W mutant, showing tryptophan side chains and anomalous-difference density in (IrCl6)3– soaked crystals. The graph serves to visualize these structural analyses and their relevance to anion binding and the K163W mutation effects.

3.4.3. H206A gain-of-function mutations:

The incorporation of the H206A mutation (identified from 6BBF pdb), equivalent to the gain-of-function H134A mutation in human Orai1, Yeung et al introduced into the Orai protein. Subsequently, they investigated the functional characteristics of the purified channel, designated as H206A Oraicryst, within proteoliposomes for activity assessment (as outlined in Figure 27)(50), (114),(109).Under conditions lacking divalent ions, which enhance the visibility of ionic currents through CRAC channels due to the superior conductance of monovalent cations (like Na+ or K+) compared to Ca^{2+}, we observed a robust influx of K+ ions through the channel(114). Notably, no ion movement was observed in empty vesicles or through a channel devoid of the H206A mutation (referred to as WT Oraicryst), in accordance with the expectation in the absence of STIM activation (as depicted in Figure 27B)(109).Similar to the behavior of wild-type CRAC channels, the introduction of Gd3+ resulted in the blockage of K+ flux (as demonstrated in Figure 27C)(109). Additionally, the K+ flux through H206A Oraicryst was hindered by the presence of Mg2+ or Ca^{2+} ions (as shown in Figure 27C), aligning with the characteristics typically exhibited by STIM-activated channels and underscoring the channel's preference for Ca^{2+} ions(50). Hence, consistent with the findings for the corresponding H134A mutation in human Orai1, the H206A Oraicryst configuration forms an open channel that effectively mimics the properties associated with STIM activation(109).

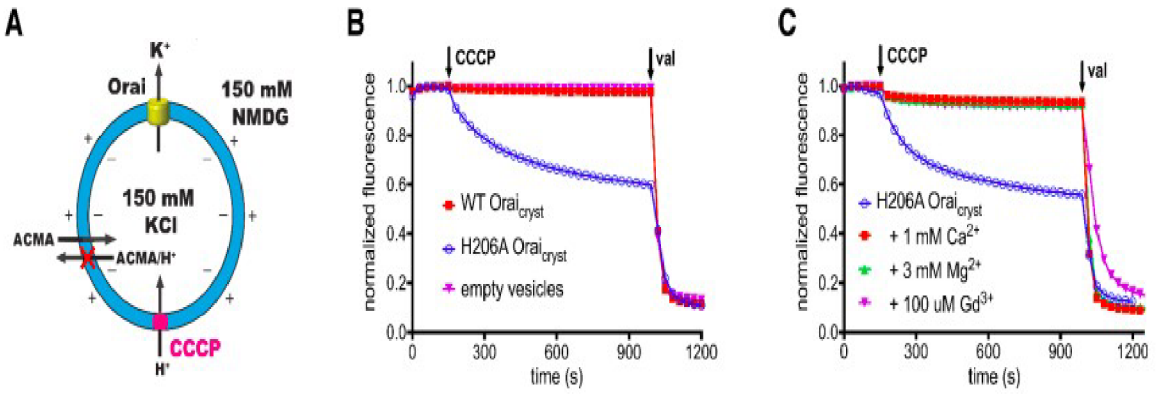

Figure 27:Ion flux through H206A Oraicryst in liposomes.(a).The schematic depicts the experimental arrangement. Vesicles containing WT or H206A Oraicryst, along with empty vesicles.(b) K+ flux measurements for H206A Oraicryst and WT are depicted. A time-dependent fluorescence decrease is observed for H206A Oraicryst following CCCP addition, indicative of K+ flux.(c) The graph highlights K+ flux inhibition through H206A Oraicryst by Ca^{2+}, Mg2+, and Gd3+.

3.4.4.Gating conformational changes in the channel:

The transitions from the closed to open states of the channel encompass rigid-body movements, where the M1–M4 segments of each of the six subunits shift away from the core of the pore. These shifts are particularly notable on the cytosolic side, leading to a slight inclination of subunits in that direction. Additionally, a curvature in the M4 helix at Pro 288, dividing it into M4a and M4b, induces outward displacement of the M4b helices (Figure 28 B,E) (117). His 206, a crucial amino acid for channel activation, forms hydrogen bonds and van der Waals interactions in the normal channel configuration, but a mutation (H206A) disrupts these interactions, prompting an open state in the absence of STIM (Figure 28 D,E,F)(101),(117). Interestingly, in the OraiH206A structure, the open state doesn't involve substantial modifications in side chain conformation, both within the pore and in other parts of the channel (101), (117). This is evident when comparing amino acid configurations in Figure 28. Since Orai subunits lack interdigitation and the α-helices align nearly perpendicular to the membrane, the movement of individual subunits remains relatively autonomous (117)

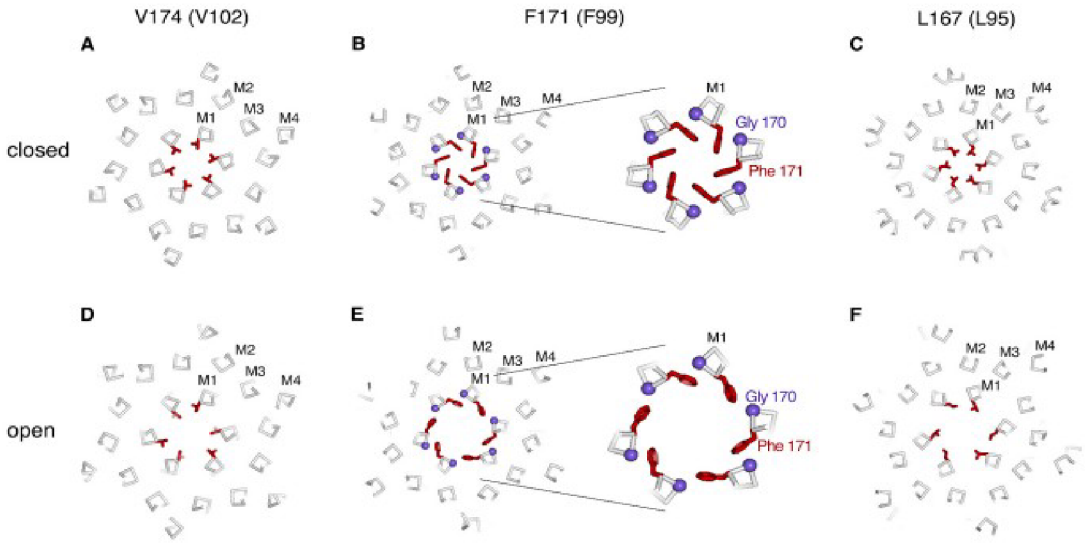

Figure 28:The graph depicts conformational changes in the hydrophobic gate, comparing slices through the closed (PDB 4HKR) and open OraiH206A structures(A-F). Close-up views highlight altered pore dimensions near Phe 171. Structures are shown as ribbons, with hydrophobic region amino acid side chains in dark red sticks, and Gly 170 as a blue sphere. The perspectives are from the extracellular side, perpendicular to the centrally located pore. The slices represent approximately 4 Å slabs centered at Val 174, Phe 171, and Leu 167, revealing outward rigid body movements of subunits. Videos provide further insight into these changes.

4. Conclusion:

In this thesis, a comparison is made between Orai1 R91C and Orai1 R91C+H134A mutations. The H134 mutation is associated with a human mutation. The Orai1-H134A mutant, which exhibits constant activity, maintained significant Ca^{2+} selectivity even without the presence of STIM1(88). Gating was instigated through heightened flexibility in the cytosolic pore portion, while the selectivity filter section became more inflexible(88). The flexibility of the pore helix was modified by introducing a H134A mutation that disrupted hydrogen bonds(96).To empirically discern differences within the pores of wild-type Orai1 and Orai1-H134A channels, a systematic cysteine scanning strategy was employed, utilizing both wild-type Orai1 and Orai1-H134A. By precisely crosslinking cysteines at distinct residues within TM1, evidence was amassed concerning their close proximity within the channel pore(112). This investigation was conducted within the context of a cysteine-free environment for both Orai1 and Orai1-H134A, which facilitated the assessment of dimerization extent. The introduction of Cu^{2+}-phenanthroline to initiate cysteine crosslinking revealed that the cysteine-free iterations of Orai1 and Orai1-H134A remained as monomers. However, the introduction of single cysteine substitutions led to the emergence of both monomeric and dimeric bands, with the occurrence contingent upon the precise position of the substitution within the channel(Figure 28 G-D)(101).

As depicted in Figure 20, the R91C+H134 mutation results in an open channel, with a strong bond observed in the 25 KDA region but no clear bond in the 50 KDA region, indicating a lack of dimerization. On the other hand, the comparison with R91C shows clear bonds in both the 25 KDA and 50 KDA regions, suggesting dimerization for R91C.

Using an alternate approach, PyMOL was employed to investigate the K163W mutant in Drosophila Orai (4HKS pdb), which corresponds to the R91W mutation in the human variant(103). This mutation induces a disorder resembling severe combined immune deficiency by hindering channel activation, thus emulating the closed channel state observed in the Orai1 mutation. Additionally, another pdb entry (6BBF) associated with Drosophila was utilized, showcasing the H206A gain-of-function mutation that mirrors the open channel structure resembling the Orai1-H134A open conformation. This allowed for an alignment to uncover both similarities and differences between the closed and open states. To conclude, the behavior of the K163W mutation in Drosophila mirrors that of the human wildtype Orai1, representing the closed conformation. Furthermore, the H206A mutation identified in Drosophila emulates the behavior of the Orai1-H134A open conformation.

The cryo-EM analysis of OraiH206A's structure (6BBF pdb) uncovers an open channel configuration. In contrast to numerous other cation channels, the process of opening in OraiH206A

lacks the involvement of twisting, bending of transmembrane helices, or substantial rotation along helical axes (115). Instead, the mechanism of opening is defined by the collective outward movement of subunits as rigid bodies. It's worth noting that the structural arrangements of amino acids in the transmembrane region remain akin in both the closed and open states (66). Impressively, this open channel structure closely corresponds to the amino acids identified for pore formation based on cysteine accessibility experiments(66)

5. References:

1. Berridge MJ, Lipp P, Bootman MD. The ver-satility and universality of calcium signalling. Nat Rev Mol Cell Biol 2000;1:11–21.Characterization of EF–SAM

2 Berridge MJ, Bootman MD, Roderick HL.Calcium signalling: dynamics, homeostasis and remodelling. Nat Rev Mol Cell Biol 2003;4:517–529.

3 .A.J. VerkhA. Lis, S. Zierler, C. Peinelt, A. Fleig, and R. Penner, "A single lysine in the N-terminal region of store-operated channels is critical for STIM1-mediated gating," J. Gen. Physiol., vol. 136, no. 6, pp. 673–686, Dec. 2010.ratsky, O.H. Petersen, Cell Calcium, 24, (1998), 333– 343.

4 .M.J. Berridge, Neuron, 21, (1998), 13– 26.

5.Putney JW. Capacitative calcium entry: from concept to molecules. Immunol Rev. 2009;231:10–22.

6.Carafoli E. Calcium signaling: a tale for all seasons. Proc Natl Acad Sci U S A.

7. Berridge MJ. The endoplasmic reticulum: a multifunctional signaling organelle. Cell Calcium 2002;32:235–249.

8.Feske S, et al. A mutation in Orai1 causes immune deficiency by abrogating CRAC channel function. Nature 2006;441:179–185.

9.B. Alberts, A. Johnson, J. Lewis, M. Raff, K. Roberts, and P. Walter, "Ion Channels and the Electrical Properties of Membranes," 2002.

10.Feske S. Calcium signalling in lymphocyte activation and disease. Nat Rev Immunol 2007;7:690–702.

11.Draber P, Draberova L. Lifting the fog in 2+store-operated Ca entry. Trends Immunol 2005;26:621–624.

12.Parekh AB, Putney JW Jr. Store-operated calcium channels. Physiol Rev 2005;85:757–810.

13. Parekh AB, Penner R. Store depletion and calcium influx. Physiol Rev 1997;77: 901–930.

14.D. E. Clapham, "TRP channels as cellular sensors," Nature, vol. 426, no. 6966, pp.517–524, Dec. 2003.

15. M. Prakriya and R. S. Lewis, "Store-Operated Calcium Channels.," Physiol. Rev., vol. 95, no. 4, pp. 1383–436, Oct. 2015.1383–436, Oct. 2015.

16.M. Hoth and R. Penner, "Calcium release-activated calcium current in rat mast cells.,"J. Physiol., vol. 465, pp. 359–86, Jun. 1993.

17.R. Penner, G. Matthews, and E. Neher, "Regulation of calcium influx by second messengers in rat mast cells," Nature, vol. 334, no. 6182, pp. 499–504, Aug. 1988.

18.S. Srikanth, B. Ribalet, and Y. Gwack, “Regulation of CRAC channels by protein interactions and post-translational modification.,” Channels (Austin)., vol. 7, no. 5, pp.354–63, 2013.
19.P. J. Shaw, B. Qu, M. Hoth, and S. Feske, “Molecular regulation of CRAC channels and their role in lymphocyte function.,” Cell. Mol. Life Sci., vol. 70, no. 15, pp. 2637–56, Aug. 2013.
20.M. A. Spassova, J. Soboloff, L.-P. He, W. Xu, M. A. Dziadek, and D. L. Gill, “STIM1 has a plasma membrane role in the activation of store-operated Ca^{2+} channels,” Proc. Natl. Acad. Sci., vol. 103, no. 11, pp. 4040–4045, Mar. 2006.
21.S. L. Zhang, A. V Yeromin, J. Hu, A. Amcheslavsky, H. Zheng, and M. D. Cahalan,“Mutations in Orai1 transmembrane segment 1 cause STIM1-independent activation of Orai1 channels at glycine 98 and channel closure at arginine 91.,” Proc. Natl. Acad. Sci. U. S. A., vol. 108, no. 43, pp. 17838–43, Oct. 2011.
22.P. G. Hogan and A. Rao, “Store-operated calcium entry: Mechanisms and modulation.,” Biochem. Biophys. Res. Commun., vol. 460, no. 1, pp. 40–9, Apr. 2015.
23.M. D. Cahalan, “STIMulating store-operated Ca(2+) entry.,” Nat. Cell Biol., vol. 11,no. 6, pp. 669–77, Jun. 2009.
24. Stathopulos PB, Ames JB, Ikura M. Structural aspects of calcium binding proteins and their interaction with targets. In: Krebs J, Michalak M, eds. CALCIUM: A Matter of Life or Death. Amsterdam: Elsevier B.V. Publishers, 2007:95–123.
25. Kretsinger RH, Nockolds CE. Carp muscle calcium-binding protein. II. Structure determination and general description. J Biol Chem 1973;248:3313–3326.
26. Ikura M. Calcium binding and conformational response in EF-hand proteins. Trends Biochem Sci 1996;21:14–17.
27. Lewit-Bentley A, Rety S. EF-hand calcium binding proteins. Curr Opin Struct Biol 2000;10:637–643.
28. Linse S, Helmersson A, Forsen S. Calcium binding to calmodulin and its globular domains. J Biol Chem 1991;266:8050–8054.
29. Ikura M, Clore GM, Gronenborn AM, Zhu G, Klee CB, Bax A. Solution structure of a calmodulin-target peptide complex by multidimensional NMR. Science 1992;256:632–638.
30. Klee CB, Ren H, Wang X. Regulation of the calmodulin-stimulated protein phosphatase, calcineurin. J Biol Chem 1998;273:13367–13370.
31. Parvez S, et al. STIM2 protein mediates distinct store-dependent and store-independent modes of CRAC channel activation.FASEB J 2008;22:752–761.
32. Bauer MC, O’Connell D, Cahill DJ, Linse S. Calmodulin binding to the polybasic C-termini of STIM proteins involved in store-operated calcium entry. Biochemistry 2008;47:6089–6091.

33.. Spassova MA, Soboloff J, He LP, Xu W, Dziadek MA, Gill DL. STIM1 has a plasma membrane role in the activation of store- operated Ca(2+) channels. Proc Natl Acad Sci USA 2006;103:4040–4045.

34. Soboloff J, Spassova MA, Tang XD, Hewavitharana T, Xu W, Gill DL. Orai1 and STIM reconstitute store-operated calcium channel function. J Biol Chem 2006;281:9.

35. Mignen O, Thompson JL, Shuttleworth TJ.2+STIM1 regulates Ca entry via arachido 2+nate-regulated Ca -selective (ARC) channels without store depletion or translocation to the plasma membrane. J Physiol 2007;579:703–715.

36.Williams RT, Senior PV, Van Stekelenburg L, Layton JE, Smith PJ, Dziadek MA. Stromal interaction molecule 1 (STIM1), a transmembrane protein with growth suppressor activity, contains an extracellular SAM domain modified by N-linked glycosylation. Biochim Biophys Acta 2002;1596: 131–137.

37. Williams RT, et al. Identification and characterization of the STIM (stromal interaction molecule) gene family: coding for a novel class of transmembrane proteins. Biochem J2001;357:673–685.

38.Matthew J. Novelloa, Jinhui Zhua,Qingping Fenga,Mitsuhiko Ikurab,Peter B. Stathopulos.Structural elements of stromal interaction molecule function.Cell calcium 73 (2018) 88-94

39.Zheng L., Stathopulos P.B., Li G.Y., Ikura M. Biochem. Biophys. Res. Commun., 369 (2008), pp. 240-246

40. Cai X. Molecular evolution and functional divergence of the Ca^{2+} sensor protein in store-operated Ca^{2+} entry: stromal interaction molecule. PLoS ONE 2007;2:e609.

41. Soboloff J, Spassova MA, Dziadek MA, Gill DL. Calcium signals mediated by STIM and Orai proteins–a new paradigm in interorganelle communication. Biochim Biophys Acta 2006;1763:1161–1168

42. Luik RM, Wu MM, Buchanan J, Lewis RS.Ca^{2+} The elementary unit of store-operated Caentry: local activation of CRAC channels by STIM1 at ER-plasma membrane junctions.J Cell Biol 2006;174:815-825.

43. Varnai P, Toth B, Toth DJ, Hunyady L, Balla T. Visualization and manipulation of plasma membrane-endoplasmic reticulum contact
sites indicates the presence of additional molecular components within the STIM1-Orai1 Complex. J Biol Chem 2007;282:29678–29690.

44.Liou J, Fivaz M, Inoue T, Meyer T. Live-cell imaging reveals sequential oligomerization and local plasma membrane targeting of stromal interaction molecule 1 after Ca^{2+} store depletion. Proc Natl Acad Sci USA 2007;104:9301–9306.

45.S. Feske et al., “A mutation in Orai1 causes immune deficiency by abrogating CRAC channel function,” Nature, vol. 441, no. 7090, pp. 179–185, May 2006.
46.S. L. Zhang, A. V Yeromin, J. Hu, A. Amcheslavsky, H. Zheng, and M. D. Cahalan,“Mutations in Orai1 transmembrane segment 1 cause STIM1-independent activation of Orai1 channels at glycine 98 and channel closure at arginine 91.,” Proc. Natl. Acad. Sci. U. S. A., vol. 108, no. 43, pp. 17838–43, Oct. 2011.
47.M. Vig et al., “CRACM1 is a plasma membrane protein essential for store-operated Ca^{2+} entry.,” Science, vol. 312, no. 5777, pp. 1220–3, May 2006.
48.M. Prakriya and R. S. Lewis, “Store-Operated Calcium Channels.,” Physiol. Rev., vol. 95, no. 4, pp. 1383–436, Oct. 2015.
49.M. J. Berridge, “Inositol trisphosphate and calcium signalling mechanisms,” Biochim. Biophys. Acta - Mol. Cell Res., vol. 1793, no. 6, pp. 933–940, Jun. 2009.
50.X. Hou, L. Pedi, M. M. Diver, and S. B. Long, “Crystal Structure of the Calcium Release-Activated Calcium Channel Orai,” Science (80-.)., vol. 338, no. 6112, pp. 1308–1313, Dec. 2012.
51.W. Ji et al., “Functional stoichiometry of the unitary calcium-release-activated calcium channel,” Proc. Natl. Acad. Sci., vol. 105, no. 36, pp. 13668–13673, Sep. 2008.
52.T. J. Shuttleworth, “Orai3--the ‘exceptional’ Orai?,” J. Physiol., vol. 590, no. 2, pp. 241–57, Jan. 2012.
53.M.Fahrner, I.Derler, I.Jardin, and C. Romanin,"The STIM1/Orai signaling machinery",Oct.2013.
54.X. Wang et al., “Distinct Orai-coupling domains in STIM1 and STIM2 define the Orai-activating site,” Nat. Commun., vol. 5, no. 1, p. 3183, Dec. 2014.
55.A. Lis, S. Zierler, C. Peinelt, A. Fleig, and R. Penner, “A single lysine in the N-terminal region of store-operated channels is critical for STIM1-mediated gating,” J. Gen. Physiol., vol. 136, no. 6, pp. 673–686, Dec. 2010.
55.I. Derler et al., “Increased Hydrophobicity at the N Terminus/Membrane Interface Impairs Gating of the Severe Combined Immunodeficiency-related ORAI1 Mutant,” J. Biol. Chem., vol. 284, no. 23, pp. 15903–15915, Jun. 2009.
56.B. S. Rothberg, Y. Wang, and D. L. Gill, “Orai Channel Pore Properties and Gating by STIM: Implications from the Orai Crystal Structure,” Sci. Signal., vol. 6, no. 267, p.pe9-pe9, Mar. 2013.
56.M. Muik et al., “Dynamic Coupling of the Putative Coiled-coil Domain of ORAI1 with STIM1 Mediates ORAI1 Channel Activation,” J. Biol. Chem., vol. 283, no. 12, pp. 8014–8022, Mar. 2008.
57.F. M. Ashcroft, “From molecule to malady,” Nature, vol. 440, no. 7083, pp. 440–447, Mar. 2006.
58.J. Soboloff, B. S. Rothberg, M. Madesh, and D. L. Gill, “STIM proteins: dynamic calcium signal transducers.,” Nat. Rev. Mol. Cell Biol., vol. 13, no. 9, pp. 549–65, Sep. 2012.

59.R. Palty, C. Stanley, and E. Y. Isacoff, "Critical role for Orai1 C-terminal domain and TM4 in CRAC channel gating.," Cell Res., vol. 25, no. 8, pp. 963–80, Aug. 2015.
60.P. B. Stathopulos et al., "STIM1/Orai1 coiled-coil interplay in the regulation of storeoperated calcium entry," Nat. Commun., vol. 4, no. 1, p. 2963, Dec. 2013.
61.R. Palty, C. Stanley, and E. Y. Isacoff, "Critical role for Orai1 C-terminal domain and TM4 in CRAC channel gating.," Cell Res., vol. 25, no. 8, pp. 963–80, Aug. 2015.
62.C. Y. Park et al., "STIM1 Clusters and Activates CRAC Channels via Direct Binding of a Cytosolic Domain to Orai1," Cell, vol. 136, no. 5, pp. 876–890, Mar. 2009.
63.L. Tirado-Lee, M. Yamashita, and M. Prakriya, "Conformational Changes in the Orai1 C-Terminus Evoked by STIM1 Binding," PLoS One, vol. 10, no. 6, p. e0128622, Jun.2015.
64.I. Frischauf et al., "Molecular determinants of the coupling between STIM1 and Orai channels: differential activation of Orai1-3 channels by a STIM1 coiled-coil mutant.," J. Biol. Chem., vol. 284, no. 32, pp. 21696–706, Aug. 2009.
65.R. Palty and E. Y. Isacoff, "Cooperative Binding of Stromal Interaction Molecule 1 (STIM1) to the N and C Termini of Calcium Release-activated Calcium Modulator 1 (Orai1).," J. Biol. Chem., vol. 291, no. 1, pp. 334–41, Jan. 2016.
66.B. A. McNally, A. Somasundaram, A. Jairaman, M. Yamashita, and M. Prakriya, "The C- and N-terminal STIM1 binding sites on Orai1 are required for both trapping and gating CRAC channels.," J. Physiol., vol. 591, no. 11, pp. 2833–50, Jun. 2013.
67.I. Frischauf et al., "A calcium-accumulating region, CAR, in the channel Orai1 enhances Ca(2+) permeation and SOCE-induced gene transcription.," Sci. Signal., vol.8, no. 408, p. Ra131, 2015.
68.R. Schindl et al., "Plasticity in Ca^{2+} selectivity of Orai1/Orai3 heteromeric channel.,"Proc. Natl. Acad. Sci. U. S. A., vol. 106, no. 46, pp. 19623–8, Nov. 2009.
69.Boehm, C., 1989. Use of polymerase chain reaction for diagnosis of inherited disorders. Clinical Chemistry, 35(9), pp.1843-1848.
70.Lorenz T. C. (2012). Polymerase chain reaction: basic protocol plus troubleshooting and optimization strategies. Journal of visualized experiments : JoVE, (63), e3998. https://doi.org/10.3791/3998
71.2020. [online] Available at: <https://www.sigmaaldrich.com/technical-documents/protocols/biology/competent-cells.html> [Accessed 31 March 2020].
72.Assets.thermofisher.com.2020.[online]Available at:<https://assets.thermofisher.com/TFS-Assets/BID/brochures/dna-isolation-purification-row-brochure.pdf> [Accessed 23 March 2020].

73.At.promega.com. 2020. [online] Available at: <https://at.promega.com/-/media/files/resources/protocols/technical-bulletins/101/pureyield-plasmid-miniprep-system-protocol.pdf?la=en> [Accessed 23 March 2020].

74.Desjardins, P., & Conklin, D. (2010). NanoDrop microvolume quantitation of nucleic acids. Journal of visualized experiments : JoVE, (45), 2565. https://doi.org/10.3791/2565

75.SOLMEGLAS Biotecnología. 2020. Transfection, Types Of Transfection And Our Customer's Favourite-Lipotransfectin.[online]: <https://solmeglas.com/transfection/> [Accessed 12 March 2020].

76.Carter, M. and Shieh, J., 2010. Guide To Research Techniques In Neuroscience. Burlington,MA: Academic Press, pp.245-247.

77.Brown, R. and Audet, J., 2008. Current techniques for single-cell lysis. Journal of The Royal Society Interface.

78.Thermofisher.com. 2020. Cell Lysis Solutions | Thermo Fisher Scientific - UK. [online] Available at: <https://www.thermofisher.com/at/en/home/life-science/protein-biology/protein-biology-learning-center/protein-biology-resource-library/pierce-protein-methods/cell-lysis-solutions.html> [Accessed 20 March 2020].

79.Rockland-inc.com. 2020. [online] Available at: <https://rockland-inc.com/Western-Blotting-Protocol.aspx> [Accessed 14 March 2020].

80. 2020. [online] Available at: <https://www.sigmaaldrich.com/catalog/product/sigma/s3401?lang=de&region=AT>[Accessed 20 March 2020].

81.Assets.thermofisher.com. 2020. [online] Available at:<http://assets.thermofisher.com/TFS-Assets/BID/Handbooks/protein-gel-electrophoresis-technical-handbook.pdf> [Accessed 20 March 2020].

82.Selva, Erica & Stronach, Beth. (2007). Germline Clone Analysis for Maternally Acting Drosophila Hedgehog Components. Methods in molecular biology (Clifton, N.J.). 397. 129-44.10.1007/978-1-59745-516-9_11.

83.Nature.com. 2020. Western Blot | Learn Science At Scitable. [online] Available at: <https://www.nature.com/scitable/definition/western-blot-288/> [Accessed 21 March2020].

84.Mahmood, T., & Yang, P. C. (2012). Western blot: technique, theory, and trouble shooting. North American journal of medical sciences, 4(9), 429–434. https://doi.org/10.4103/1947-2714.100998

85.2020. [online] Available at: <https://www.sigmaaldrich.com/technical-documents/protocols/biology/western-blotting.html> [Accessed 21 March 2020].

86. Hou, X.; Pedi, L.; Diver, M.M.; Long, S.B. Crystal structure of the calcium release-activated calcium channel Orai. Science 2012, 338, 1308–1313, doi:10.1126/science.1228757.

87. Yeromin, A.V.; Zhang, S.L.; Jiang, W.; Yu, Y.; Safrina, O.; Cahalan, M.D. Molecular identification of the CRAC channel by altered ion selectivity in a mutant of Orai. Nature 2006, 443, 226–229, doi:10.1038/nature05108.

88. McNally, B.A.; Somasundaram, A.; Yamashita, M.; Prakriya, M. Gated regulation of CRAC channel ion selectivity by STIM1. Nature 2012, 482, 241–245, doi:10.1038/nature10752.

89.Feske, S. Immunodeficiency due to defects in store-operated calcium entry. Ann. N. Y. Acad. Sci. 2011, 1238, 74–90, doi:10.1111/j.1749-6632.2011.06240.x.

90.F. M. Ashcroft, Ion channels and disease : channelopathies. Academic Press, 2000.

91.Derler, I., M. Fahrner, O. Carugo, M. Muik, J. Bergsmann, R. Schindl, I.Frischauf, S. Eshaghi, and C. Romanin. 2009. Increased hydropho-bicity at the N-terminus/membrane interface impairs gating of theSCID-related ORAI1 mutant. J. Biol. Chem. https://doi.org/10.1074/jbc.M808312200

92.McNally, B.A., M. Yamashita, A. Engh, and M. Prakriya. 2009. Structuraldeterminants of ion permeation in CRAC channels. Proc. Natl. Acad. Sci.USA. 106:22516–22521. https://doi.org/10.1073/pnas.0909574106

93.Zhang, S.L., A.V. Yeromin, J. Hu, A. Amcheslavsky, H. Zheng, and M.D. Ca-halan. 2011. Mutations in Orai1 transmembrane segment 1 causeSTIM1-independent activation of Orai1 channels at glycine 98 and channelclosure at arginine 91. Proc. Natl. Acad. Sci. USA. 108:17838–17843.https://doi.org/10.1073/pnas.1114821108

94.Yeung, P.S., M. Yamashita, C.E. Ing, R. Pomès, D.M. Freymann, and M.Prakriya. 2018. Mapping the functional anatomy of Orai1 transmem-brane domains for CRAC channel gating. Proc. Natl. Acad. Sci. USA. 115:E5193–E5202. https://doi.org/10.1073/pnas.1718373115

95.X.Hou,L.Pedi,M.Diver,SB.Long,Nov 2012.Crystal Structure of the Calcium Release–Activated Calcium Channel Orai.[Online]. Available at:https://www.science.org/

96.Frischauf I, Litviňuková M, Schober R, Zayats V, Svobodová B, Bonhenry D, Lunz V, Cappello S, Tociu L, Reha D, Stallinger A, Hochreiter A, Pammer T, Butorac C, Muik M, Groschner K, Bogeski I, Ettrich RH, Romanin C, Schindl R. Transmembrane Helix connectivity in Orai1 controls two Gates for calcium-dependent transcription. Science Signaling. 2017;10:eaao0358. doi: 10.1126/scisignal.aao0358.

97.Kane Dickson V, Pedi L, Long SB. Nature. 2014 Dec 11 .Structure and insights into the function of a Ca(2+)-activated Cl(-) channel.;516(7530):213-8. doi: 10.1038/nature13913. Epub 2014 Oct 22.

98.Stephen K. Burley, Helen M. Berman, Gerard J. Kleywegt, John L. Markley, Haruki Nakamura & Sameer Velankar.(2017).Protein Data Bank (PDB): The Single Global Macromolecular Structure Archive

99.S Yuan, HCS Chan, Z Hu - Wiley Interdisciplinary Reviews 2017 Using PyMOL as a platform for computational drug design
100.V Raj, A Raj, D Kumar, V Kumar - PharmaTutor, 2015 Molecular Modeling Studied for Inhibition of Calcium Channel Receptor: A Strategy for the development of new Antiepileptic Drug,[Online]pharmatutorjournal.com
101.I Frischauf, M Litviňuková, R Schober, V Zayats… - Science …, 2017 - science.org,Transmembrane helix connectivity in Orai1 controls two gates for calcium-dependent transcription
102.B. S. Barker, G. T. Young, C. H. Soubrane, G. J. Stephens, E. B. Stevens, and M. K. Patel, “Ion Channels,” Conn’s Transl. Neurosci., pp. 11–43, Jan. 2017.
103.Tiffner,A.,Maltan,L.,Derler,I., 2021.The Orai Pore Opening Mechanism
104. C Guardiani, D Sun, A Giacomello - Frontiers in Molecular ,2021 ,Unveiling the gating mechanism of CRAC channel: a computational study,Available at: frontiersin.org
105.Hou, X., Pedi, L., Diver, M., and Long, S. (2012). Crystal Structure of the Calcium Release-Activated Calcium Channel Orai. Science 338, 1308–1313. doi:10.1126/science.1228757.
106..G. M. Cooper, The cell : a molecular approach. ASM Press, 2000.
107.Y Li, X Yang, Y Shen - 2021 – researchgate.net,Structural Insights into Ca^{2+} Permeation through Orai Channels.
108.M.Prakriya, S.Feske ,Y.Gwack, S.Srikanth, A.Rao, PG.Hogan .(2006).Orai1 is an essential pore subunit of the CRAC channel
109.X. Hou, S.R. Burstein, S.B. Long Structures reveal opening of the store-operated calcium channel Orai Elife, 7 (2018).
110.Dong H, Fiorin G, Carnevale V, Treptow W, Klein ML: Pore waters regulate ion permeation in a calcium release-activated calcium channel. Proc Natl Acad Sci U S A 2013, 110:17332
111.Frischauf I, Zayats V, Deix M, Hochreiter A, Jardin I, Muik M, Lackner B, Svobodova B, Pammer T, Litvinukova M, Sridhar AA, et al. A calcium-accumulating region, CAR, in the channel Orai1 enhances Ca(2+) permeation and SOCE-induced gene transcription. Sci Signal. 2015;8:ra131.
112.Zhou Y, Ramachandran S, Oh-Hora M, Rao A, Hogan PG. Pore architecture of the ORAI1 store-operated calcium channel. Proc Natl Acad Sci U S A. 2010;107:4896–4901.
113.A Amcheslavsky, ML Wood, AV Yeromin, I Parker .Molecular biophysics of Orai store-operated Ca^{2+} channels.Biophysical journal, 2015 – cell.com
114.Yeung PS, Yamashita M, Ing CE, Pome` s R, Freymann DM, Prakriya M. 2018. Mapping the functional anatomy of Orai1 transmembrane domains for CRAC channel gating. PNAS 115:E5193–E5202. DOI: https://doi.org/10.

115.Jiang Y, Lee A, Chen J, Cadene M, Chait BT, MacKinnon R. 2002b. The open pore conformation of potassium channels. Nature 417:523–526. DOI: https://doi.org/10.1038/417523a, PMID: 12037560

116.Online source information for Pymol,https://pymolwiki.org/.

117.X Hou, IR Outhwaite, L Pedi, SB Long, Cryo-EM structure of the calcium release activated calcium channel Orai in an open conformation.